SYNAPTIC PLASTICITY RULES AT CA3–CA3 RECURRENT SYNAPSES IN HIPPOCAMPUS

by

Rajiv Kumar Mishra

March, 2016

A thesis presented to the
Graduate School
of the
Institute of Science and Technology (IST) Austria, Klosterneuburg, Austria
in partial fulfillment of the requirements
for the degree of
Doctor of Philosophy

The dissertation of Rajiv Kumar Mishra, titled **"**Synaptic Plasticity Rules at CA3–CA3 Recurrent Synapses in Hippocampus"**,** is approved by:

Supervisor: Prof. Dr. Peter Jonas, IST Austria, Klosterneuburg, Austria

Signature: _____

Committee Member: Prof. Dr. Jozsef Csicsvari, IST Austria, Klosterneuburg, Austria

Signature: _____

Committee Member: Prof. Dr. Michael Frotscher, Institute for Structural Neurobiology, Center for Molecular Neurobiology, University of Hamburg, Germany

Signature: _____

Defense Chair: Dr. Vladimir Kolmogorov, IST Austria, Klosterneuburg, Austria

Signature: _____

I hereby declare that this dissertation is my own work, and it does not contain other people's work without this being so stated, that this thesis does not contain my previous work without this being stated, and that the bibliography contains all the literature that I used in writing the dissertation.

I declare that this is a true copy of my thesis, including any final revisions, as approved by my thesis committee, and that this thesis has not been submitted for a higher degree to any other university or institution.

Signature: _____

Rajiv Kumar Mishra

Abstract

CA3 pyramidal neurons are thought to play a key role in memory storage and pattern completion by activity-dependent synaptic plasticity between CA3–CA3 recurrent excitatory synapses. To examine the induction rules of synaptic plasticity at CA3–CA3 synapses, we performed whole-cell patch-clamp recordings in acute hippocampal slices from rats (postnatal 21–24 days) at room temperature. Compound excitatory postsynaptic potentials (EPSPs) were recorded by tract stimulation in *stratum oriens* in the presence of 10 µM gabazine. High-frequency stimulation (HFS) induced N-methyl-D-aspartate (NMDA) receptor-dependent long-term potentiation (LTP). Although LTP by HFS did not require postsynaptic spikes, it was blocked by Na^+-channel blockers suggesting that local active processes (e.g. dendritic spikes) may contribute to LTP induction without requirement of a somatic action potential (AP).

We next examined the properties of spike timing-dependent plasticity (STDP) at CA3–CA3 synapses. Unexpectedly, low-frequency pairing of EPSPs and backpropagated action potentials (bAPs) induced LTP, independent of temporal order. The STDP curve was symmetric and broad, with a half-width of ~150 ms. Consistent with these specific STDP induction properties, post–presynaptic sequences led to supralinear summation of spine [Ca^{2+}] transients. Furthermore, in autoassociative network models, storage and recall was substantially more robust with symmetric than with asymmetric STDP rules.

In conclusion, we found associative forms of LTP at CA3–CA3 recurrent collateral synapses with distinct induction rules. LTP induced by HFS may be associated with dendritic spikes. In contrast, low frequency pairing of pre- and postsynaptic activity induced LTP only if EPSP–AP were temporally very close. Together, these induction mechanisms of synaptic plasticity may contribute to memory storage in the CA3–CA3 microcircuit at different ranges of activity.

This thesis is dedicated to my beloved grandparents.

‘For every step, the footprint was already there.’

Roberto Calasso

About the Author

Born and brought up in India, Rajiv started his scientific journey in 2003 at Banaras Hindu University, where he studied chemistry for his bachelor's degree. He then moved to Jawaharlal Nehru University, Delhi, where he obtained a master's degree in biotechnology. He was involved in a short project with Prof. Dr. Neeraj Jain at National Brain Research Centre, Manesar, where he studied structural plasticity post traumatic injury in Macaque monkeys. At last, for his PhD, he joined Prof. Dr. Peter Jonas at IST Austria, where he dedicated himself to studying synaptic plasticity in CA3 pyramidal neurons in hippocampus. His paper reporting on the findings was accepted for publication in Nature communications.

Acknowledgements

This PhD thesis is culmination of my deep interest in neuroscience research and has been possible by the help and support of numerous people over the years. Firstly, I would like acknowledge my supervisor Prof. Peter Jonas at IST Austria for his support, encouragement and advice throughout my PhD. Through the training in his group, I have acquired exceedingly many technical and personal skills that are vital in my career development as a researcher.

I would also like to thank Professor Jozsef Csicsvari and Professor Michael Frotscher for being my thesis committee members despite their busy schedule.

I would like to express deepest respect to my previous mentors at various stages of my career, Mr. Ranjit Dubey and Late Mr. L. B. Dixit. I would also like to thank Prof. Neeraj Jain who gave me plenty of encouragement and advice during my tenure in his lab as research assistant at National Brain Research Centre, India.

My special appreciation and thanks to Dr. Jose Guzman for his valuable suggestions and discussions throughout my PhD.

I would like to thank all my colleagues and friends in the lab. Special thanks to Michael Schunn, Eva Kramberger, Florian Marr and Sarah Rosenthaler, for their warm support and tremendous help during my stay at IST Austria.

I am also very thankful to IST Austria for their support all throughout my PhD.

Last but not the least; I would like to express my deepest gratitude to my family and friends for always supporting and encouraging me with their best wishes.

Table of contents

Lists of Publications Appearing in Thesis

Original publication

Mishra, R.K., Kim, S., Guzman, S.J., Jonas, P. Symmetric spike timing-dependent plasticity at CA3–CA3 synapses optimizes storage and recall in autoassociative networks. *Nature Communications* (in Press)

Posters and presentations

Mishra, R.K., Guzman, S.J., Jonas, P. Associative long-term potentiation at CA3–CA3 glutamatergic synapses in hippocampus. *Society for Neuroscience abstracts* 45.01 (2012).

Mishra, R.K., Jonas, P., Guzman, S.J. Associative long-term potentiation at CA3–CA3 glutamatergic synapses in the hippocampus. *GRC Synaptic Transmission* (2014).

Mishra, R. K. Cooperative and associative plasticity in glutamatergic CA3–CA3 recurrent synapses. *Neuroscience data talk, IST Austria* (2015).

I have obtained editorial permission to include the data which is originally submitted / published in Nature Communications. All the experiments shown in this thesis were conducted by me and no data from co-authors has been included.

Signature: _____

Rajiv Kumar Mishra

List of figures

Abbreviations

aCSF	artificial cerebrospinal fluid
ADP	afterdepolarization
AMPAR	α-amino-5-hydroxy-3-methyl-4-isoxazole propionic acid receptor
AP	action potential
APV	2-amino-5-phosphonovalerate
ATP	adenosine 5’-triphosphate
bAP	backpropagated action potential
CA	cornu ammonis (hippocampus)
C/A	commissural / associational
CaMK II	calcium/calmoduline -dependent kinase II
CNQX	6-cyano-7-nitroquinoxaline-2,3-dione
DAB	3,3´-diaminobenzidine
DCG-4	(2*S*,2'*R*,3'*R*)-2-(2',3'-dicarboxycyclopropyl)glycine
DG	dentate gyrus
EC	entorhinal cortex
EPSP	excitatory postsynaptic potential
Glu	glutamate
GTP	guanosine 5’-triphosphate
HFS	high-frequency stimulation
IR-DIC	infrared-differential videomicroscopy
LTP	long-term potentiation
LTD	long-term depression
mGluR	metabotropic glutamate receptor
NMDAR	N-methyl-D-aspartate receptor
PP	perforant path
PSD	postsynaptic density
STDP	spike timing-dependent plasticity
TTX	tetrodotoxin

1 Introduction

1.1 Declarative memory and hippocampus

Memory is a process in which information about an individual's environment is encoded, stored and retrieved. Memory can be divided into *procedural (implicit)* and *declarative (explicit)* memories. Procedural memory builds up slowly, through repetition over many trials and does not depend directly on conscious processes. Examples of implicit memory include perceptual and motor skills and the learning of certain types of procedures and rules (Schacter et al., 2010). Declarative memory on the other hand requires conscious recall e.g. memory of facts and verbal knowledge. It can be further divided into: *episodic* and *semantic memory. Episodic memory* is involved in storing specific personal experiences while *semantic memory* is associated with storage of factual information (Tulving, 1972).

Though nearly all brain regions play a pivotal role in some aspect of memory, the hippocampus and related areas are shown to be particularly important for declarative memory (Eichenbaum, 2001). The hippocampus is part of the limbic system located in the temporal lobe of each hemisphere. The first evidence of the role of the hippocampus on memory formation and storage came from the study on Henry Moliason, known as 'Patient H.M.', the most intensively studied subject in medical history (Squire, 2009). In their famous report, William B. Scoville and Brenda Milner (Scoville and Milner, 1957) describe the results of surgical removal of H.M.'s hippocampus in order to alleviate severe epileptic seizures. The consequence of this surgery was severe anterograde and partial retrograde amnesia. H.M. was unable to form new episodic memories (memories of events: a form of declarative memory). He could not remember the events that occurred just before his surgery leaving intact his childhood memories. It has also been reported that the hippocampus encodes spatial information. Spatial memory is a part of declarative memory responsible for recording information about one's environment and its spatial orientation (Milner et al., 1998; O'Keefe and Dostrovsky, 1971; Squire, 2004). This form of memory

helps an animal to navigate around a familiar environment. If neurons are the cellular substrate for the memory, cellular phenomena such as synaptic transmission and plasticity may explain how memories can be stored and retrieved in the hippocampus.

1.2 Hippocampal network

The hippocampus is subdivided into three subregions; the CA3 region (CA for cornu ammonis), the CA1 region, and the dentate gyrus (DG; Lorente de Nó, 1934).

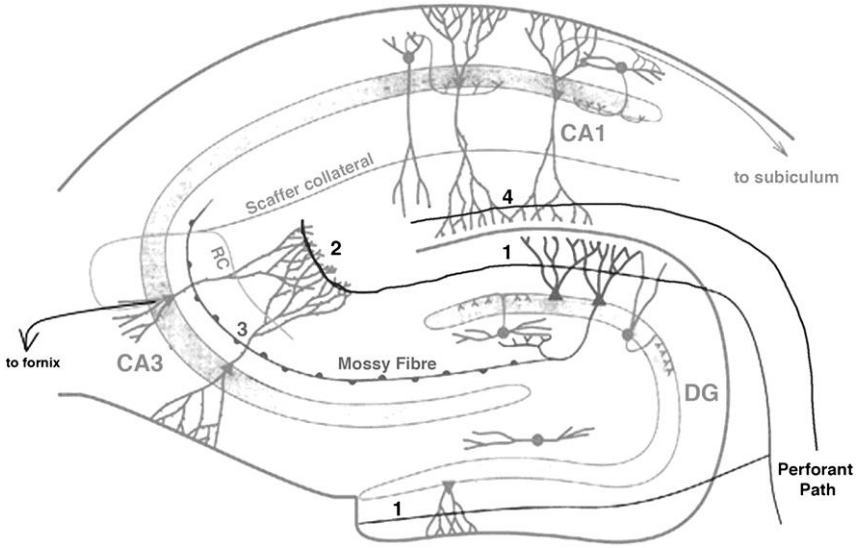

Figure 1: Schematic representations of the hippocampal excitatory pathways

(a) Perforant Pathway (PP): Layer II of the entorhinal cortex (EC) projects their axons to granule cells in dentate gyrus (1) and CA3 in pyramidal cell layer (2). Layer III of EC projects to CA1 pyramidal neurons (4).
(b) GCs send their axons (called “mossy fibers”) to CA3 (3).
(c) CA3 pyramidal neurons send their axons to either other pyramidal neurons in CA3 region (recurrent collaterals; RC) or to CA1 (Schaffer collaterals, SC).
(d) Pyramidal cells of CA1 send their axons to the subiculum and deep layers of the EC (taken from Rolls and Treves, 1998)

Each subregion consists of a population of principal neurons and numerous interneurons. The three subregions (GC→CA3→CA1) are connected in series

via excitatory synapses, forming the trisynaptic loop (Cajal, 1911; Andersen, 1975).

The entorhinal cortex projects to granule cells in the DG region and the axons of these cells further target the CA3 pyramidal neurons. The axons of the CA3 pyramidal cells send their projections to the CA1 pyramidal neurons. CA1 sends back the output of the hippocampal network to the cortex via subiculum (Amaral and Witter, 1995).

1.2.1 Granule cells

There are the approximately 10^6 granule cells in the DG region. A typical granule cell has an elliptical cell body packed together with a cone-shaped tree of spiny apical dendrites (Claiborne et al., 1990). The axons of granule cells, called mossy fibers (MFs) project to the CA3 pyramidal cell layer (Amaral et al., 1990; Chicurel and Harris, 1992, Blackstad et al., 1970; Swanson et al., 1978; Claiborne et al., 1986). MF–CA3 excitatory synapses are unique due to several features: giant presynaptic terminals, multiple transmitter release sites, prominent paired-pulse facilitation (Henze et al., 2000; Bischofberger et al., 2006) and presynaptic expression mechanisms of plasticity (Zalutsky and Nicoll, 1990; Kobayashi et al., 1996; Tzounopoulos et al., 1998).

1.2.2 CA3 pyramidal neurons

CA3 pyramidal neurons are embedded in a classical trisynaptic circuitry (Andersen et al., 1971). There are approximately 300,000 CA3 pyramidal neurons in the circuit. The main characteristic of these neurons is their complex dendritic structures called thorny excrescences (Witter 2007) and their burst firing properties (Masukawa et al., 1982).

Pyramidal cells in the CA3 region are further divided into CA3a, CA3b and CA3c. CA3 pyramidal neurons send their input to pyramidal cells in the CA1 region via Schaffer collaterals (Schaffer, 1892) and receive excitatory inputs from three different sources; (1) the MFs from granule cells, (2) the PP inputs from layer II of entorhinal cortex and (3) the recurrent collaterals of CA3 pyramidal cells (CA3–CA3 recurrent synapses, Ishizuka et al., 1990).

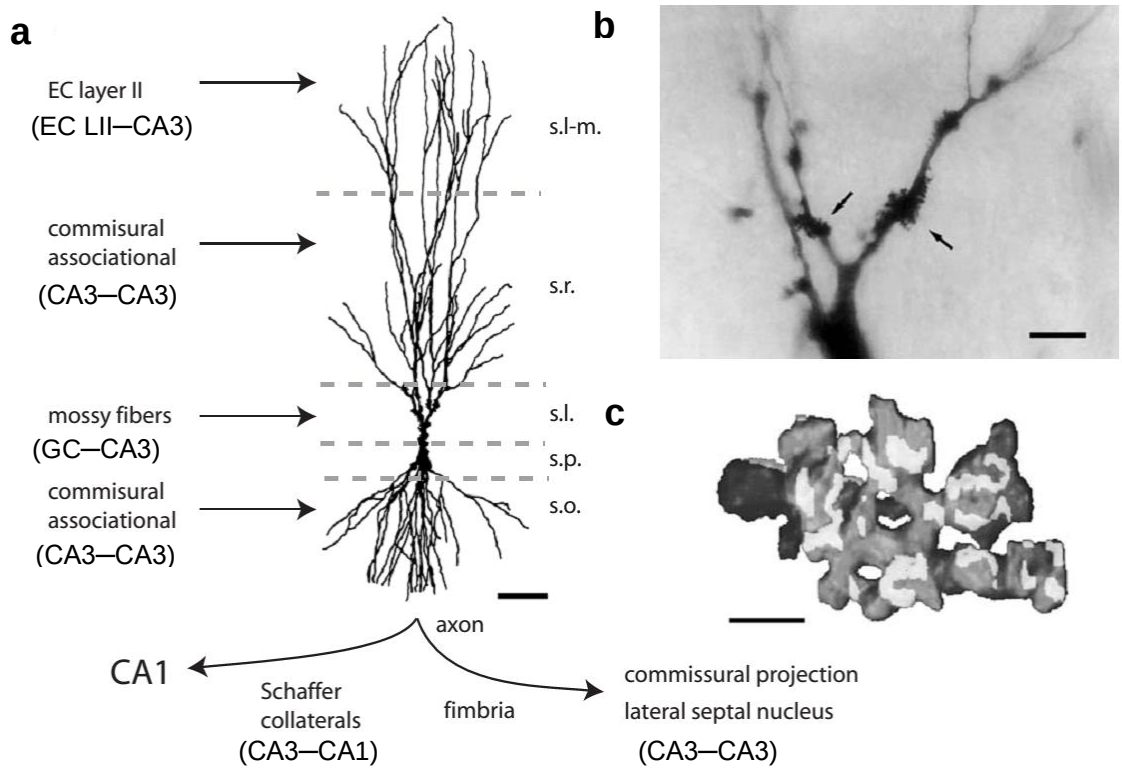

Figure 2: Schematic CA3 morphology and synaptic inputs and outputs

(a) Dendritic morphology of a CA3 pyramidal neuron. The major excitatory synaptic inputs to CA3 pyramidal neuron as well as are the major synaptic outputs. Bar 50 µm. (b) The presence of thorny excrescences (large spine clusters) on proximal apical dendrites of CA3 neurons in *stratum lucidum* (s.l.) as shown by the arrows. Bar 25 µm. (c) 3-D reconstruction of a large branched spine. The reconstructed thorn is light gray, and the PSDs are indicated in white. Bar 1 µm. (taken from Andersen et al., 2007).

CA3–CA3 recurrent synapses are the most abundant excitatory synapses in the hippocampus (Frotscher et al., 1991; Li et al., 1994). CA3 neurons also send strong commissural projections to contralateral CA3 and CA1. The excitatory synapses on CA3 neurons are monosynaptically activated by recurrent collaterals (MacVicar and Dudek, 1980; Miles and Wong, 1983, 1986). The commissural input also forms synapses with CA3 pyramidal cells, both in *stratum radiatum* and in *stratum oriens* (Andersen et al., 1969; Andersen, 1975).

Several lines of evidence suggest that CA3–CA3 recurrent synapses are the main subcellular correlates of pattern completion. First, the CA3–CA3 synaptic system is the most extensive synaptic system in the entire brain (Li et al.,

1994), providing a large capacity network to store information. Second, CA3–CA3 synapses show robust long-term plasticity, rendering them highly suitable for information storage (Zalutsky and Nicoll, 1990; Debanne et al., 1997; Montgomery et al., 2001). Third, selective genetic deletion of NMDA-type glutamate receptors in CA3 pyramidal neurons impairs pattern completion, presumably by abolishing plasticity at CA3–CA3 synapses (Nakazawa et al., 2002).

Finally, network models endowed with recurrent connectivity and Hebbian synaptic plasticity can reproduce storage, recall, and pattern completion (Marr, 1971; McNaughton and Morris, 1987; Lisman, 1999; Gibson and Robinson, 1992; Treves and Rolls, 1994; Bennett et al., 1994).

1.2.3 CA1 pyramidal neurons

CA1 pyramidal neurons are one of the most studied classes of neurons in the brain from both structural and functional points of view. The principle excitatory inputs arrive from the EC and CA3 pyramidal neurons. Schaffer collaterals (inputs from CA3 pyramidal neurons from both hemispheres) form synapses on the apical dendrites in *stratum radiatum* and on the basal dendrites in *stratum oriens* (Schaffer, 1892).

Several studies using restricted knockouts and overexpression of the NMDAR and with regulated expression of calcium-calmodulin-dependent kinase II (CaMKII) at CA3–CA1 synapses have reported that molecular pathways important for LTP are also required for spatial information processing (Tang et al., 1999; Martin et al., 2000; Morris, 2006; Mayford et al., 1996).

1.3 Activity-dependent synaptic plasticity

An activity-dependent change in the strength of synapses is termed as synaptic plasticity. “When an axon of cell A is near enough to excite a cell B and repeatedly or persistently takes part in firing it, some growth process or metabolic change takes place in one or both cells such that A’s efficiency, as one of the cells firing B, is increased” (Hebb, 1949). The theory was proposed by Hebb in his famous book “The Organization of Behavior”. In short,

simultaneous activity of two cells leads to an increase in their synaptic strengths. This forms the basis of “associative or Hebbian learning”. This theory challenged the general belief that synapses are merely a mode to transfer information between a pair of neurons or between a neuron and a muscle cell. It is now well established that the strength of most of the synapses can be changed or modified.

There are two forms of synaptic plasticity depending on whether the strength of the synapses increases or decreases: (1) long-term potentiation (LTP) and (2) long-term depression (LTD; Bliss and Lømo, 1973; Levy and Steward, 1983; Siegelbaum and Kandel, 1991; Bliss and Collingridge, 1993; Nicoll and Malenka, 1995b).

1.3.1 Long-term potentiation

An activity-dependent persistent increase in the synaptic strength is called long-term plasticity. LTP was first described in the rabbit hippocampus (Bliss and Lømo 1973). In this study presynaptic fibers of the perforant pathway were stimulated and responses were recorded from a group of postsynaptic cells in the area dentate gyrus as field excitatory postsynaptic potentials (fEPSPs). Following a high-frequency train of stimuli delivered to the presynaptic fibers, the fEPSP response of postsynaptic cells was enhanced for several hours. This phenomenon of long-lived enhancement in the synaptic strength of postsynaptic cells was termed as LTP. LTP has been observed in practically all brain areas including cerebral cortex, cerebellum and amygdala (Clugnet and LeDoux, 1990).

A direct link between LTP and learning and memory has been shown in several studies. Blocking the activity of proteins involved in synaptic plasticity either pharmacologically or through gene knockout affected animals to perform certain behaviorally relevant tasks (Lynch, 2004; Martin et al., 2000; Morris, 2006).

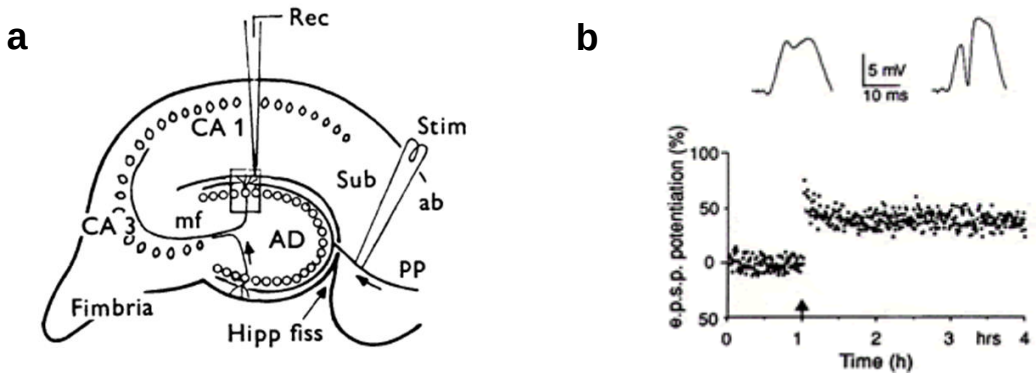

Figure 3: Experimental demonstration of LTP

(a) Schematic representation of the recording configuration. EPSPs were recorded from granule cells by performant path stimulation
(b) An increase in synaptic strength of EPSPs following high-frequency stimulation (taken from Bliss and Lømo, 1973).

Impaired spatial memory has been reported by infusing NMDAR antagonist into the hippocampus (Morris and Frey, 1997). Also, overexpression or lack of expression of specific subunits of NMDARs is shown to affect synaptic plasticity and thereby spatial memory (Tang et al., 1999).

1.3.2 Long-term depression

If potentiation would be the only process for the activity-dependent change in strength of synapses, synapses will reach their maximum efficiency at a certain time point. At this point the network would stop processing new information and therefore learning will be ceased. LTD is one of several mechanisms by which strength of synapses is weakened in order to avoid saturation of the network. LTD has been discovered in CA1 pyramidal neurons of the rat hippocampus (Dudek and Bear, 1992). The typical protocol for LTD induction consists of low frequency (0.5−5 Hz) stimulation for 900 repetitions or with a lesser number of repetitions if the postsynaptic neurons are held at a slightly depolarized membrane potential (Selig et al., 1995).

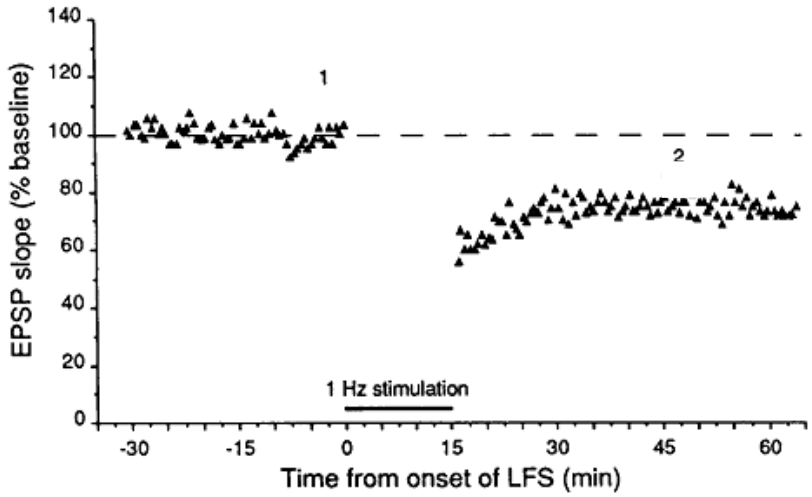

Figure 4: LTD induction by LFS

Population EPSP evoked by stimulation of the Schaffer collaterals at 0.03 Hz. The horizontal bar represents the period of 1-Hz conditioning stimulation (taken from Dudek and Bear, 1992).

Based on the mechanism, there are two different forms of LTD-(1) NMDAR-dependent, e.g. LTD at CA3–CA1 synapses (Mulkey and Malenka, 1992), (2) metabotropic glutamate receptor (mGluR)-dependent, e.g. cerebellum and cortex (Bolshakov and Siegelbaum, 1994; Oliet et al., 1997; Otani and Connor, 1998). Both mechanisms coexist in adults (Heynen et al., 1996; Oliet et al., 1997; Otani and Connor, 1998). In young animals LTD is predominantly mGluR-dependent (Bolshakov and Siegelbaum, 1994; Normann et al., 2000).

LTD has been shown to be important for encoding spatial information and thus is involved in formation of the spatial map (Kemp and Vaughan, 2007).

1.3.3 Mechanism of LTP and LTD induction

Synaptic plasticity at Schaffer collaterals synapses (CA3–CA1) is the most studied form of plasticity. LTP at CA1 pyramidal neurons requires NMDAR activation through postsynaptic depolarization (Bliss and Collingridge, 1993; Malenka and Nicoll, 1999). During basal synaptic transmission, i.e. at resting membrane potentials, synaptically released glutamate binds to both NMDARs and α-amino-5-hydroxy-3-methyl-4-isoxazole propionic acid receptors

(AMPARs). Ions flow through the AMPARs but not through the NMDARs because of the Mg^{2+} block.

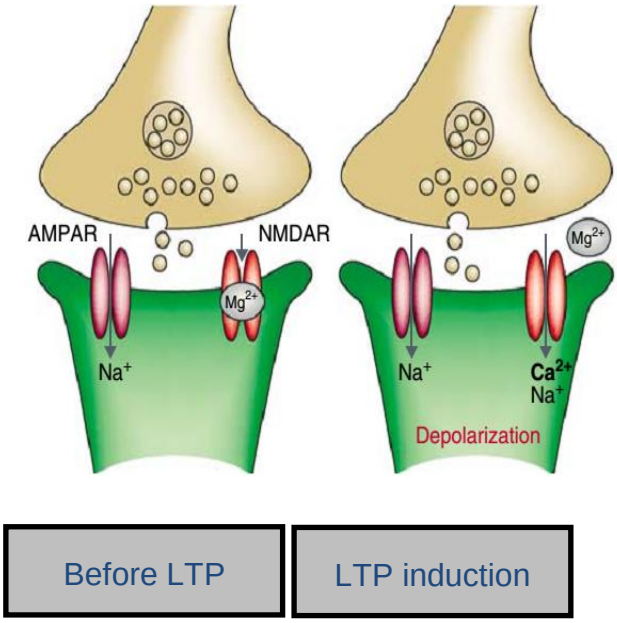

Figure 5: Model of synaptic transmission at excitatory synapses
Basal synaptic transmission (left panel). Depolarization of the postsynaptic cell leads to NMDAR activation (right panel; taken from Citri and Malenka 2008).

Depolarization of the postsynaptic cell as a result of activity of the post- and presynaptic neurons relieves the Mg^{2+} block. Subsequent activation of the NMDAR leads to an increase in Ca^{2+} concentration within the dendritic spine. This process could act as a trigger for induction of either LTP or LTD (Mulkey and Malenka, 1992). A moderate increase in Ca^{2+} leads to LTD (Cummings et al., 1996) whereas LTP occurs when the increase in Ca^{2+} crosses a certain threshold (Malenka and Nicoll, 1993).

1.3.4 Signal transduction mechanism for LTP and LTD

LTP has been shown to be prevented by blocking CaMKII (Malenka et al., 1989; Malinow et al., 1989). More direct evidence came from a study in which a knockout mouse lacking alpha-CaMKII subunit (Silva et al., 1992) did not show

LTP. In another study, LTP was prevented in an animal with CaMKII lacking the autophosphorylation site (Giese et al., 1998).

Some other kinases are also shown to be important for LTP such as cyclic adenosine monophosphate-dependent protein kinase (PKA; Blitzer et al., 1998, Lisman, 1989, Makhinson et al., 1999), extracellular signal-regulated kinase (Erk)/mitogen-activated protein kinase (MAPK) pathway (Sweatt, 2004; Thomas and Huganir, 2004), Src kinase (Kalia et al., 2004) and protein kinase C (Hrabetova and Sacktor, 1996; Ling et al., 2002, Pastalkova et al., 2006, Serrano et al., 2005).

LTD, on the other hand, involves activation of a Ca^{2+}-dependent protein phosphatase cascade. This cascade consists of the calcium / calmodulin-dependent phosphatase calcineurin / protein phosphatase 2B, PP1, and a phosphoprotein termed inhibitor-1. Inhibitor-1 inhibits PP1 until it is dephosphorylated by calcineurin (Lisman, 1989). Accordingly, LTD is abolished by application of phosphatase inhibitors (Kirkwood and Bear, 1994, Mulkey et al., 1994, 1993). In another study intracellular application of PP1 enhances LTD (Morishita et al., 2001).

1.3.5 Mechanism of LTP/LTD expression

A persistent biochemical signal described in the previous section acts upon an effector, e.g. a glutamate receptor, resulting in the expression of plasticity. Change in neurotransmitter release would suggest a presynaptic expression mechanism. A postsynaptic mechanism could be explained through changes in AMPARs properties. An increase in the numbers of AMPARs within the postsynaptic density has been reported at hippocampal CA1 synapses. Thus, LTP expression at these synapses is postsynaptic and mediated by activity-dependent changes in AMPAR trafficking (Bredt and Nicoll, 2003; Derkach et al., 2007; Malenka and Nicoll, 1999; Malinow and Malenka, 2002; Song and Huganir, 2002). It involves endocytosis of synaptic AMPARs (Bredt and Nicoll, 2003; Collingridge et al., 2004; Derkach et al., 2007; Malenka and Bear, 2004; Malinow and Malenka, 2002). Dissociation of AMPARs from their anchors within the postsynaptic density (PSD) has been reported, followed by lateral

movement to the edge of the PSD. There they undergo clathrin- and dynamin-dependent endocytosis (Ashby et al., 2004; Blanpied et al., 2002; Groc et al., 2004).

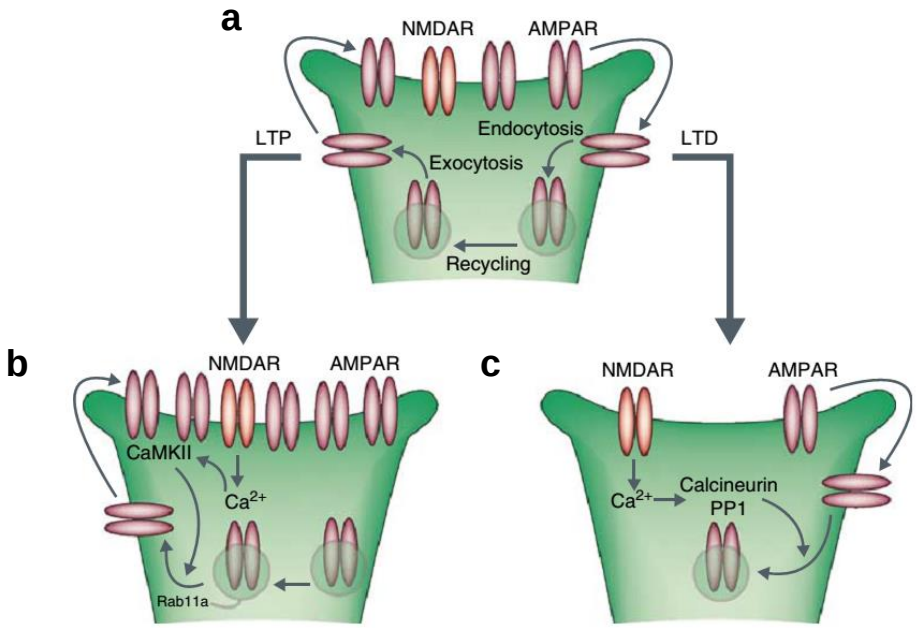

Figure 6: Model of AMPAR trafficking during LTP and LTD

(a) In the basal state, receptors cycle between the postsynaptic membrane and intracellular compartments through lateral mobility of the receptors out of the synapse into endocytic zones.
(b) Following induction of LTP, there is enhanced receptor exocytosis and stabilization at the synapse. This process is Ca^{2+}-driven and involves CAMKII and fusion of recycling endosomes mediated by Rab11a.
(c) Following the induction of LTD, enhanced endocytosis at extrasynaptic sites occurs. This process is also Ca^{2+}-dependent but involves protein phosphatases, primarily calcineurin and protein phosphatases 1 (PP1; taken from Citri and Malenka, 2008).

A postsynaptic expression of LTP can also involve a phosphorylation-driven increase in the single-channel conductance of AMPARs (Benke et al., 1998, Soderling and Derkach, 2000). A presynaptic expression mechanism on the other hand requires a retrograde messenger (brain-derived neurotrophic factor; BDNF, nitric oxide; NO). These messengers might be released by postsynaptic cells and acts on presynaptic terminals (Nicoll, 2003).

1.4 Spike timing-dependent plasticity (STDP)

Change in the strength of synapses observed by pairing presynaptic spikes with postsynaptic APs is termed as spike timing-dependent plasticity (STDP). The relevance of spike timing may vary across synapses but there is a general consensus that STDP could be the primary mechanism for Hebbian learning in several regions of the brain (Hebb, 1949; Markram et al., 1997; Magee and Johnston, 1997; Bi and Poo, 1998; Zhang et al., 1998; Sjöström et al., 2001; Feldman, 2012). In early studies, STDP (also called Hebbian STDP) was mostly bidirectional and order dependent at many excitatory synapses (Markram et al., 1997; Magee et al., 1997; Bi and Poo, 1998).

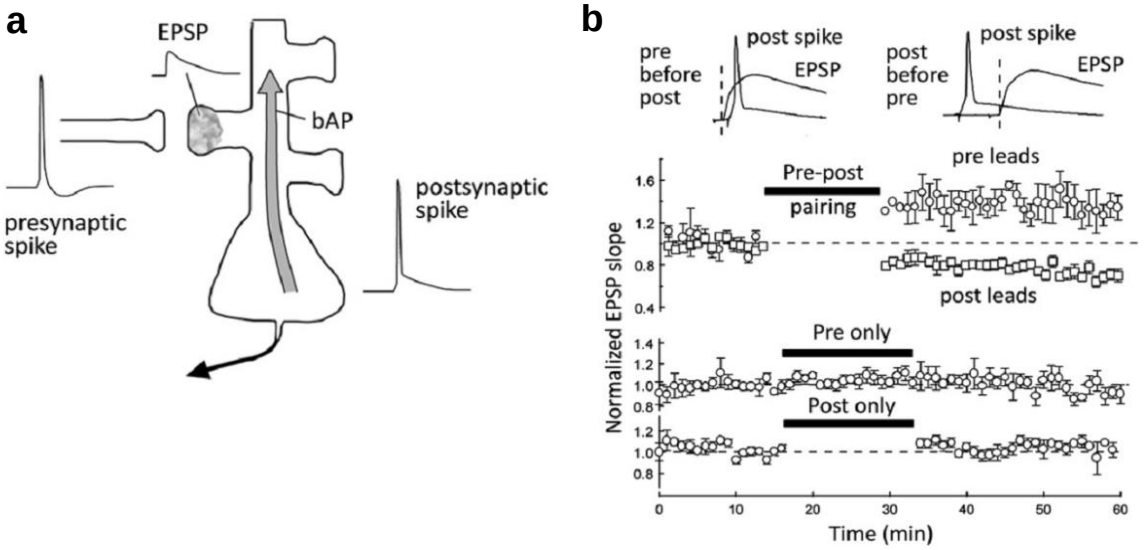

Figure 7: Spike timing-dependent plasticity

(a) Induction of STDP by pairing EPSP with postsynaptic AP
(b) Pre-before-post spiking drives LTP; while post-before-pre spiking drives LTD. Pre- or postsynaptic spikes alone do not alter synapse strength (Feldman 2000).

A pre–postsynaptic sequence of activity within a narrow time window induces LTP whereas post–presynaptic sequence of activity induces LTD. In their independent findings, Markram et al., 1997 and Magee and Johnston, 1997 showed the order dependence of synaptic plasticity. A synapse got potentiated if presynaptic stimulation occurred first whereas if postsynaptic AP was presented before presynaptic stimulation, it was depressed.

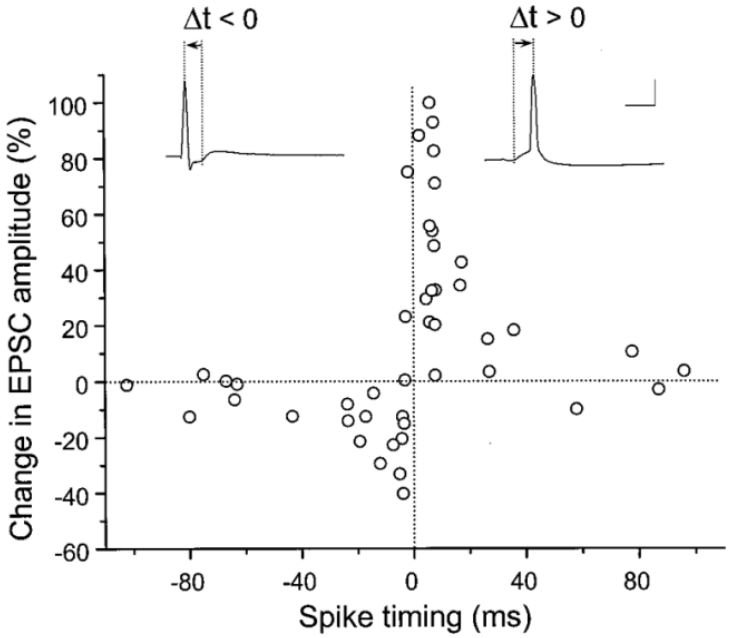

Figure 8: Critical window for the induction of LTP and LTD

Note the order dependence of STDP with a peak around 10 ms for LTP and a negative peak for LTD at –10 ms (taken from Bi and Poo, 1998).

However, a full description of the STDP was first provided by Bi and Poo in their study on cultures of dissociated rat hippocampal neurons in 1998. (Bi and Poo, 1998) They showed that postsynaptic APs that peaked within a time window of 20 ms after synaptic activation resulted in LTP. LTD occurred when the activity was reversed (spiking within a time window of 20 ms before synaptic activation). A narrow transition zone of ~5 ms existed between the LTP and LTD windows. When the time interval (Δt) of pairing was increased on either sides of pairing, no potentiation / depression was observed.

Many different forms of STDP time windows have been reported from various excitatory synapses across the brain (Feldman, 2012). In neocortex layer 5, layer 2/3 pyramidal neurons and hippocampal CA1 pyramidal neurons the STDP is balanced between LTP and LTD.

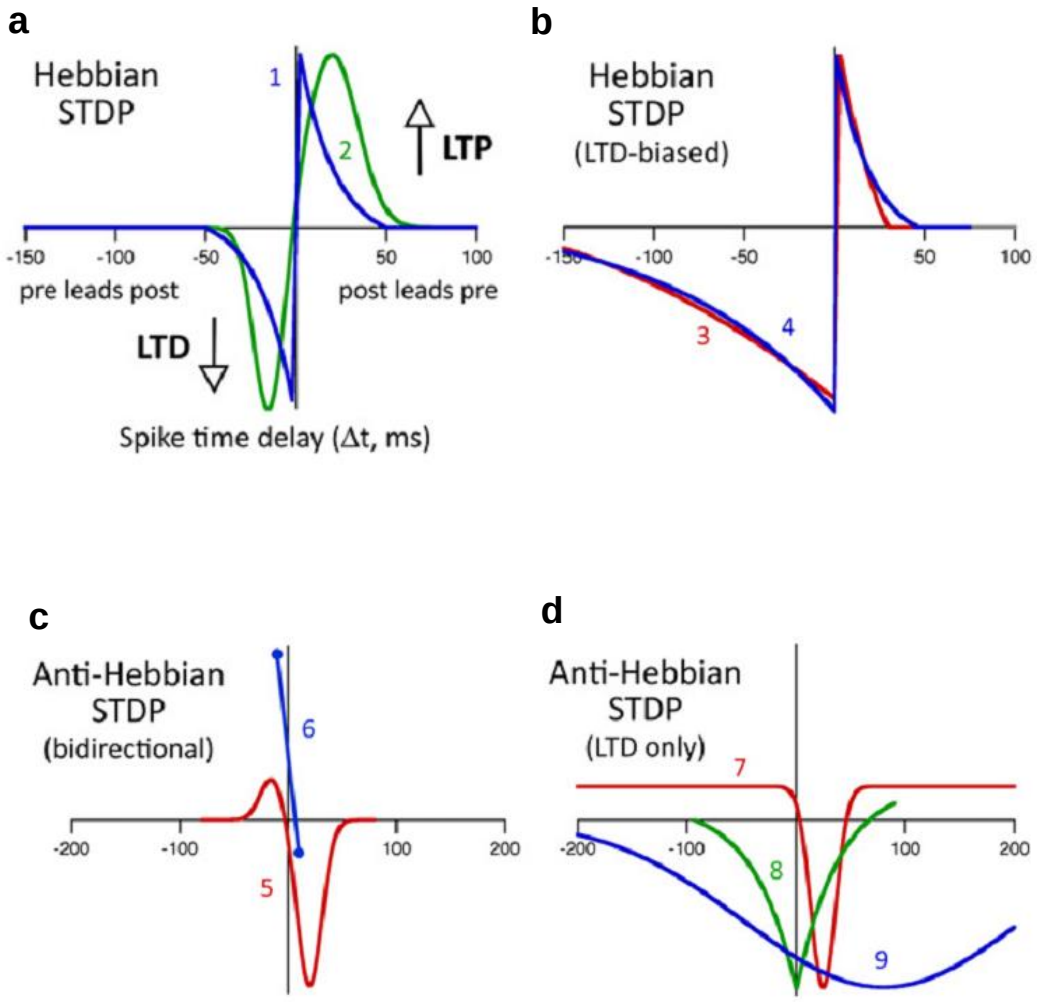

Figure 9: STDP exist in different forms

(a) Hebbian STDP that is equally balanced between LTP and LTD. 1- Froemke et al., 2005; 2- Fino et al., 2008.
(b) Hebbian STDP that is biased toward LTD. 3- Celikel et al., 2004; 4- Froemke et al., 2005.
(c) Anti-Hebbian STDP that contains both LTP and LTD. 5- Fino et al., 2005;
6- Letzkus et al., 2006.
(d) Anti-Hebbian STDP that contains only LTD (anti-Hebbian LTD). 6- Han et al., 2000; 7- Lu et al., 2007; 8- Safo and Regehr, 2008 (taken from Feldman 2012).

STDP also varies by postsynaptic cell type in *striatum* (Fino et al., 2008, 2009). Neuromodulation and dendritic depolarization also play a key role in shaping the order / amplitude of synaptic plasticity. For instance, dopamine and inhibition affect the sign of STDP in hippocampal and striatal neurons (Fino et

al., 2005; Shen et al., 2008; Zhang et al., 2009). Manipulations which either depolarize the dendrites or make bAP more effective are able to change the direction of STDP from LTP to LTD or vice versa (Sjöstrom and Häusser, 2006; Letzkus et al., 2006; Zilberter et al., 2009).

There are other factors which might influence STDP apart from spike timing. These factors include firing rate, synaptic cooperativity, and postsynaptic voltage (Markram et al., 1997; Sjöstrom et al., 2001).

1.5 Aim of the study

CA3 pyramidal neurons in the hippocampal network play a key role in spatial information processing and memory. These neurons are embedded in the classical trisynaptic circuitry (Andersen et al., 1971), but also give origin to commissural / associational (C/A) synapses, the most abundant glutamatergic synapses in the hippocampus (Li et al., 1994). Classical network models suggest a major role of these synapses in spatial learning (Marr, 1971). For example, synaptic plasticity at these synapses is believed to be of key importance for pattern completion (Nakazawa et al., 2002). However, synaptic plasticity rules at these synapses have not been determined yet in acute hippocampal preparations.

To clarify the role of CA3–CA3 cell synapses in learning and memory, we systematically analyzed synaptic plasticity at these synapses. We employed electrophysiological recordings, single spine Ca^{2+} imaging and network simulations to answer the following questions:

(1) Are these synapses plastic, i.e. whether an activity-dependent change in synaptic strength is possible?
(2) If so, is plasticity associative and how is plasticity dependent on spike timing?
(3) What are the mechanisms driving plasticity?
(4) What is the functional relevance of plasticity at the network level?

2 Materials and methods

2.1.1 Brain dissection and slice preparation

Transverse hippocampal slices (thickness, 350 µm) were prepared from the brains of 21- to 24-day-old Wistar rats of either sex (Kim et al., 2012). Animals were lightly anesthetized using isofluorane (Forane®; Abbott) and sacrificed by rapid decapitation. Experiments were performed in strict accordance with institutional, national, and European guidelines for animal experimentation and were approved by the Bundesministerium für Wissenschaft, Forschung und Wirtschaft (A. Haslinger, Vienna). Slices were cut in ice-cold sucrose-containing physiological saline using a vibratome (VT1200, Leica Microsystems), incubated in a maintenance chamber filled with sucrose-saline at ~36°C for ~45 min, and subsequently stored at room temperature. Slices were then individually transferred into a recording chamber perfused with standard physiological saline. Recordings were performed at room temperature (~22°C, range: 21–23°C) or near-physiological temperature (~33°C; range 32–34°C) as indicated. In the experiments at ~33°C, temperature was controlled using a water jacket or a temperature controller (Sigmann Elektronik, Hüffenhardt, Germany). Slices were used for maximally six hours after dissection.

2.1.2 Electrophysiology

Patch pipettes were pulled from thick-walled borosilicate glass tubing (outer diameter: 2 mm, inner diameter: 1 mm) using a horizontal pipette puller (P-97, Sutter Instruments). When filled with internal solution, the open-tip resistance was 4–6 MΩ. All measurements were performed with an Axoclamp 700B amplifier (Molecular Devices). Signals were low-pass filtered at 5–10 kHz and digitized at a sampling rate of 20 kHz with a CED 1401 plus interface (Cambridge Electronic Design). Pulse protocols were generated using custom-made data acquisition software (FPulse 3.33; U. Fröbe, Freiburg) running under Igor Pro 6.22 (WaveMetrics) and Signal 6 (Cambridge Electronic Design). Whole-cell patch-clamp recordings were made from the soma of visually

identified pyramidal neurons located in the *stratum pyramidale* of the CA3b subfield (Fig. 1a). Resting membrane potential was measured immediately after membrane rupture.

EPSPs were recorded in the presence of 10 µM SR-95531 (gabazine). To stimulate input synapses, a borosilicate glass pipette (2–3 MΩ) filled with 1 M sodium chloride (NaCl) was placed in *stratum oriens* (~200 µm away from the soma of the recorded CA3 pyramidal cell). As axons of CA3 pyramidal neurons often traverse the pyramidal cell layer, this location will activate synapses on both apical and basal dendrites of target cells (Li et al., 1994; Ropireddy et al., 2011), while avoiding stimulation of mossy fiber inputs. Axons were stimulated with brief voltage pulses (3–25 V amplitude, 100 µs duration) via a stimulus isolation unit at a basal frequency of 0.1–0.2 Hz. Stimulus intensity was chosen to give evoked EPSP amplitude of 1–5 mV, corresponding to ~2–10 unitary synaptic inputs (Guzman et al., 2014b).

To verify the selective stimulation of CA3–CA3 recurrent synapses, the effect of bath application of DCG-4 (1 µM; an agonist of type II mGluRs) was tested at the end of the experiment in the majority of recordings. DCG-4 inhibits mossy fiber synaptic transmission substantially (Kamiya et al., 1996). Cells were excluded from further analysis if DCG-4 inhibited evoked EPSPs by >15%, which would indicate contamination by mossy fiber synapses.

To confirm the identity of the recorded neurons, a subset of cells was filled with biocytin during recording and labeled using 3, 3'-diaminobenzidine (Kim et al., 2012). All labeled neurons showed the typical morphology of CA3 pyramidal neurons, including a high density of spines on their dendritic branches.

For EPSP recording, series resistance was fully compensated, and pipette capacitance was ~70% compensated. Both resting membrane potential and input resistance (R_{in}) of the recorded CA3 pyramidal neuron were monitored over time. Experiments were discarded if the resting membrane potential depolarized above –60 mV, R_{in} fell below 100 MΩ, or R_{in} changed by more than 30% during the recording. Membrane potential values were specified without correction for liquid junction potentials.

2.1.3 Induction of synaptic plasticity

LTP was induced with either pairing or HFS paradigms.

(1) The HFS protocol consisted of 4 trains of 100 stimuli at 100 Hz delivered every 10 s.

(2) The pairing protocol consisted of 300 repetitions of a single presynaptic stimulation paired with a postsynaptic AP at different time intervals at 1 Hz. APs were evoked by brief current injection (4 nA amplitude, 2 ms duration) to the soma.

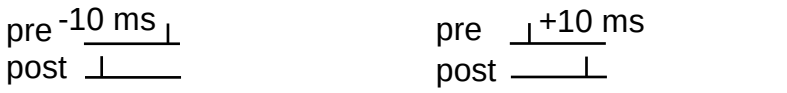

Post–presynaptic sequence Pre–postsynaptic sequence

2.1.4 Single spine Ca^{2+} imaging

Imaging of CA3 pyramidal neuron spines was performed using an upright microscope (DM 6000 FS, Leica Microsystems) equipped with a confocal laser scanhead (TCS SP5 II, Leica Microsystems) using either a 20x (NA = 1.0) or a 63x (NA = 0.9) water immersion objective. Before imaging, neurons in the CA3b area were identified with Infrared-differential interference contrast (IR-DIC) microscopy using a CCD camera (DFC365 FC, Leica Microsystems). CA3 pyramidal neurons were loaded with 100 µM of the Ca^{2+} indicator dye Fluo-5F and 50 µM of the Ca^{2+}-insensitive dye Alexa Fluor 594 (both Invitrogen) via the patch pipette (Oertner et al., 2002). To allow for a proper equilibration of the dyes, fluorescence signals were measured 40–50 min after break-in, and series resistance was kept below 25 MΩ. Excitation wavelength was 488 nm (argon laser) for Fluo-5F and 561 nm for Alexa Fluor 594 (diode pumped solid state laser).

To detect spines that responded to the stimulation of the recurrent CA3 recurrent synapses, we scanned an area of 11.5 x 11.5 µm with 10 frames (128 x 128 pixels) acquired at a rate of 3.9 Hz while a stimulation electrode was placed in the vicinity of a dendrite (typically < 20 µm). Reactive spines were identified by an increase in the green fluorescence in the presence of a

modified Mg^{2+}-free physiological saline. In total, ~5% of spines were reactive. For subsequent recording, standard physiological saline was used.

For imaging, regions of interest were set to basal dendrites 50–200 µm from the soma. Line scans of spines, dendrites, or both were acquired every 400 Hz. Distance of reactive spines was measured as the shortest linear path along the dendrite from the scanning site to the tip of the somatic pipette. Fluorescent transients were recorded in response to extracellular synaptic stimulation or bAPs evoked by brief somatic current pulses (4 nA, 2 ms), both delivered every 15 s. All recordings were made in the presence of 10 µM gabazine in the bath solution. Intracellular [Ca^{2+}] transients were analyzed with custom-made routines implemented in Fiji (Schindelin et al., 2012) and were expressed as green over red ratio, $\Delta G(t)/R = (G(t) - G_0)/R$, where $G(t)$ is the fluorescence time course in the green channel, G_o is the mean basal fluorescence signal 50 ms before stimulation, and R is the mean fluorescence signal of the red channel during the acquisition time (Oertner et al., 2002). No background subtraction was performed, but care was taken to avoid dye ejection from the patch pipette during cell approach and sealing procedure. [Ca^{2+}] transients shown in figures represent average fluorescence of 5–10 consecutive line scans including failure, unless noted differently.

2.1.5 Solutions and chemicals

Sucrose-based solution was used for dissection and storage of slices that contained 87 / 64 mM NaCl, 25 mM $NaHCO_3$, 2.5 mM KCl, 1.25 mM NaH_2PO_4, 7 mM $MgCl_2$, 0.5 mM $CaCl_2$, 25 mM glucose, and 75 / 120 mM sucrose. Physiological saline for experiments (artificial cerebrospinal fluid, aCSF) contained 125 mM NaCl, 25 mM $NaHCO_3$, 2.5 mM KCl, 1.25 mM NaH_2PO_4, 1 mM $MgCl_2$, 2 mM $CaCl_2$, and 25 mM glucose. Slices were superfused at a rate of 2.5–5.0 ml min^{-1} (recording chamber volume ~2 ml). For current-clamp recording, intracellular solution was composed of 140 mM K-gluconate, 20 mM KCl, 10 mM HEPES, 0.1 mM EGTA, 2 mM $MgCl_2$, 4 mM Na_2ATP, and 0.3 mM NaGTP, pH adjusted to 7.28 with KOH (~300 mOsm). For imaging, intracellular solution contained 135 mM K-gluconate, 20 mM KCl, 10 mM HEPES, 2 mM $MgCl_2$, 4 mM Na_2ATP, 0.3 mM NaGTP, 2 mM ascorbic acid, 50 µM Alexa Fluor

594, and 100 µM Fluo-5F, pH adjusted to 7.28 with KOH (~300 mOsm). In subsets of experiments, 10 mM phosphocreatine was included (effect was unnoticeable).

Extracellularly applied chemicals were kept in concentrated stock solution in ultrapure water at –20°C and dissolved in physiological saline immediately before the experiment. These included: D-AP5 (D-2-amino-5-phosphonovaleric acid), nimodipine (3-(2-methoxyethyl) 5-propan-2-yl 2,6-dimethyl-4-(3-nitrophenyl)-1,4-dihydropyridine-3,5-dicarboxylate), DCG-4 ((2*S*,2'*R*,3'*R*)-2-(2',3'-dicarboxycyclopropyl)glycine), Tetrodotoxin (TTX) and SR-95531 (2-(3-carboxypropyl)-3-amino-6-(4 methoxyphenyl) pyridazinium bromide; gabazine). Intracellularly applied EGTA (ethylene glycol-bis (2- aminoethylether)-N,N,N´,N´-tetraacetic acid) and QX-314 (*N*-(2,6-dimethylphenyl-carbamoylmethyl) triethylammonium chloride) were directly added to the pipette solution and were allowed to diffuse into the recorded cell for ~20 min before the experiment was started.

2.1.6 Data analysis

Analysis of evoked EPSPs was performed with Stimfit (version 0.13 or 0.14; Guzman et al., 2014a) or equivalent custom-made routines written in C or Python 2.6 or 2.7. The rise time of the EPSPs was determined as the time interval between the points corresponding to 20 and 80% of the peak amplitude, respectively. The peak amplitude was determined as the mean or maximum within a window of 1 or 2 ms duration, respectively, following the stimulus. The synaptic latency was determined as the time interval between the center of the stimulus artifact and the onset of the subsequent EPSP; the onset point was determined from the intersection of a line through the 20 and 80% points with the baseline. The decay phase of the EPSPs was fit with a monoexponential function using a nonlinear least-squares fit algorithm. To assure reliable quantification of LTP, only recordings with stationary baseline, as tested by a Spearman rank-correlation test ($P > 0.05$), were included. The magnitude of LTP was quantified by ratio between the mean EPSPs amplitude

20−30 min after the induction paradigm and the mean value in a 10-min time interval before induction.

2.1.7 Storage and recall in autoassociative network models

Simulations of pattern completion in autoassociative network models were performed following previous work (Supplementary Table 1). The network was implemented with a size of 3,000 neurons, connected by excitatory synapses with a probability of 0.5. For each storage cycle (e.g. a theta cycle of 200 ms duration), synaptic plasticity was implemented using different STDP rules based on piecewise exponential functions. In the symmetric rule (Fig. 4b, top), the potentiation function was $y(\Delta t) = \text{Exp}[-\text{Abs}(\Delta t) / \tau_{pot}]$, where Δt is the time difference between EPSP and AP, τ_{pot} is the time constant, and Abs is the absolute value. τ_{pot} was set to one time unit, corresponding to one storage cycle. In the asymmetric rule (Fig. 4b, bottom), the potentiation function was $y(\Delta t) = \text{Sign}(\Delta t) \times \text{Exp}[-\text{Abs}(\Delta t) / \tau_{pot}]$, where Sign is the signum function. Basal synaptic strength (j_0) was assumed as 0. The total activity level a was set to 0.1. Activity in the network was assumed to show normally distributed spike times, with a standard deviation σ_t of 0.2 time units, which would correspond to a 20%-fraction of a storage cycle. The lower and upper boundaries for synaptic efficacy were 0 and 1, respectively.

Neuronal activity during progressive recall was simulated during 5–10 time steps. Excitatory synaptic potentials in the network were generated according to the function $v(t, \delta) = \text{Step}(t - \delta) \times \text{Exp}[-(t - \delta)/ \tau_{syn}]$, where δ is a delay determined by the spike time of the presynaptic neuron, and τ_{syn} is the synaptic decay time constant (1 time unit, corresponding to one recall cycle, e.g. a theta, gamma, or ripple cycle), For each recall cycle, the total input to the i^{th} neuron at time t was calculated as $h_i(t) = \frac{1}{n} \sum_{j=1}^{n} W_{ij}\ J_{ij}\ v(t, T_j)$, where W denotes the connectivity matrix, J represents synaptic potentiation matrix, Tj is the spike time of the j^{th} presynaptic neuron in the previous recall cycle (–infinity for silent neurons), and n is the number of neurons. A neuron was assumed to fire action potentials in a given recall cycle if the condition $h_i(t) - \frac{1}{n}\ g_1 S \geq g_0$ was met, where S is the total activity in the network in the prior cycle, g_0 is the firing threshold (set to 0), and g_1 is the proportionality factor of inhibition

(varied between 0 and 1). The spike time was calculated by solving the equation $h_i(T) - \frac{1}{n} g_1 S = g_0$. Retrieval was tested with incomplete random patterns, in which the proportion of valid firing neurons was 0.5 (i.e. $b_1 = 0.5$), and the proportion of spuriously firing neurons was 0 (i.e. $b_n = 1$). The overlap between original and recalled patterns was computed as the correlation coefficient between original and final activity vectors. The absolute capacity of the network was defined as the maximum of the product function of pattern correlation times pattern load. The capacity of the implemented 3,000-neuron network was up to 100 patterns, but was substantially increased for real-sized 330,000-neuron networks (P.J., unpublished observations). Simulations were implemented in Mathematica, Matlab, C, or C++, and run on PCs or a scientific computer cluster (Supermicro, San Jose, CA, USA) using GNU/Debian Linux (x86_64), a GNU C compiler (GCC, 4.9.2), and the GNU scientific library (GSL, 1.16). Computer code will be provided upon request.

2.1.8 Statistics and conventions

All values are given as mean ± SEM. Error bars in the figures also indicate SEM (shown only if larger than symbol size). Statistical significance was tested using a two-sided Wilcoxon signed rank test for paired data or a two-sided Wilcoxon rank sum test for unpaired data (Igor Pro 6.3.2). Differences with $P < 0.05$ were considered significant. Throughout the figures, * indicates $P < 0.05$, ** $P < 0.01$, and *** $P < 0.001$.

3 Results

3.1 Characteristics of CA3-CA3 recurrent synapses

CA3 pyramidal neurons were identified based on the following criteria, (a) location in the slice, (b) electrophysiological properties such as firing pattern, AP phenotype and input resistance (R_{in}), and (c) morphology, e.g. presence of thorny excrescences and characteristic axonal arborization in *post hoc* biocytin labeling of the CA3 pyramidal neuron (Fig. 10a, b). We next examined whether the kinetic properties of CA3–CA3 recurrent synapses are consistent with their proposed function in storage and recall and studied synaptic plasticity of these synapses in acute hippocampal slices from mature rats (21 -24 day old Wistar rats).

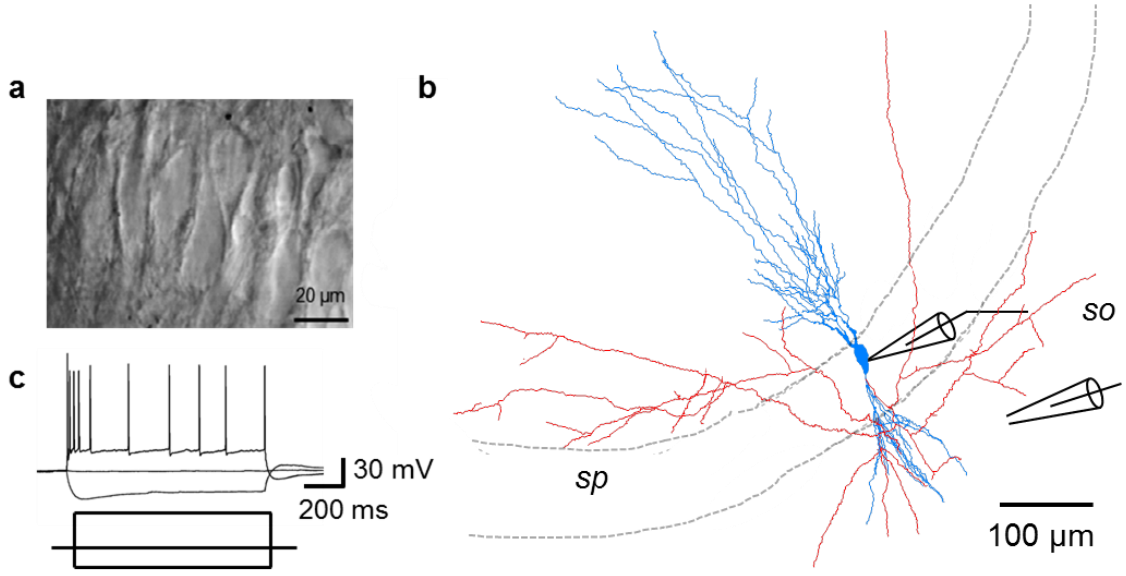

Figure 10: Cellular identification of CA3 pyramidal neurons

(a) IR-DIC image of the CA3b area of an acute slice preparation of the rat hippocampus.
(b) Neurolucida reconstruction of a CA3 pyramidal neuron filled with biocytin. Recording and stimulation pipettes are indicated schematically. Blue, soma and dendrites; red, axon; sp, *stratum pyramidale*; so, *stratum oriens*.
(c) Voltage response of a CA3 pyramidal neuron to a depolarizing (630 pA) and hyperpolarizing (-250 pA) current injection.

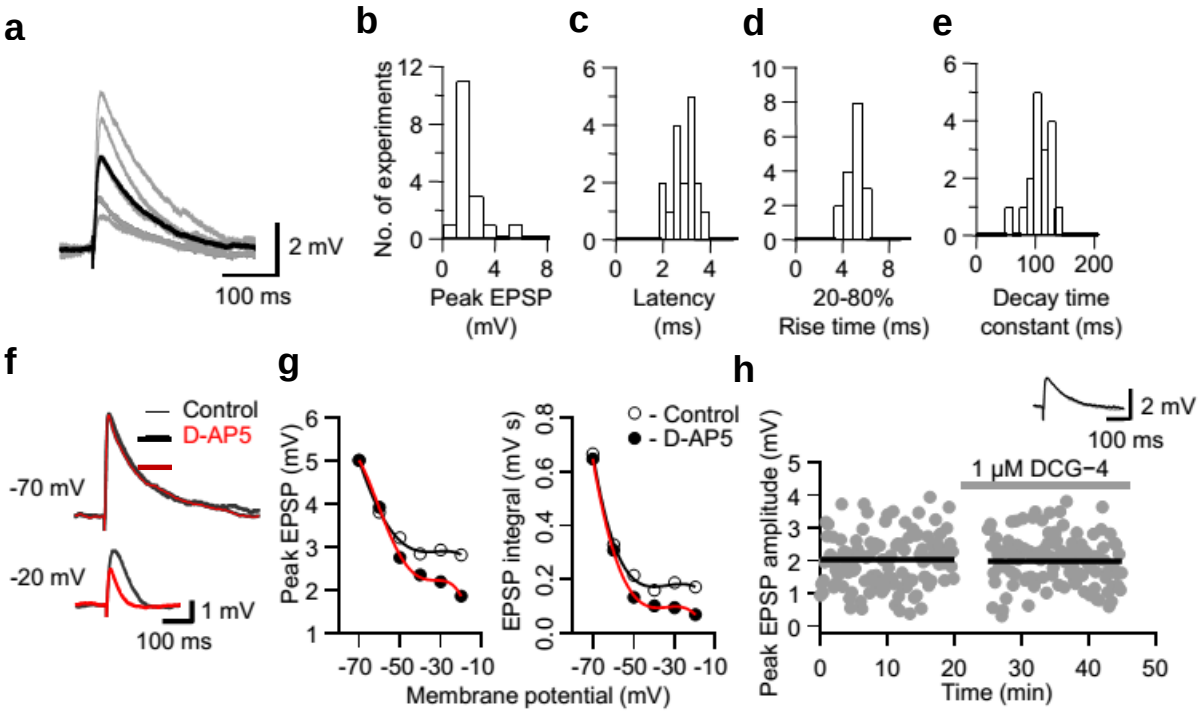

Figure 11: Properties of compound EPSPs at hippocampal CA3–CA3 synapses

(a) EPSPs were isolated by extracellular stimulation of the recurrent collaterals in the presence of 10 µM gabazine. Single EPSPs traces are shown in gray and the average is shown in black.
(b–e) Histograms of peak EPSP amplitude (b), latency (c), 20–80% rise time (d) and decay time constant of EPSPs (e, 17 cells).
(f) EPSP traces in control (drug-free) conditions (black) and in the presence D-AP5 (red) at –70 mV (top) and –20 mV. To prevent spiking at more depolarized holding potentials, 5 mM QX-314 was added to the pipette solution. A slower voltage component was blocked at depolarizing holding potential was abolished by D-AP5 indicating a NMDAR component.
(g) Plot of EPSP peak amplitude (left) and integral (right) against holding potential. Open symbols, data in control; filled symbols, data in the presence of 20 µM D-AP5. Red curves represent 5-th order polynomial functions fit to the data points.
(h) Plot of compound EPSP peak amplitude against experimental time during application of 1 µM of DCG-4 (horizontal bar). Note that DCG-4 has no significant effects on basal synaptic response suggesting selective stimulation of CA3–CA3 cell synapses. Inset shows overlay of average EPSP traces in control conditions and in the presence of DCG-4 (black and gray, respectively).

Recurrent collaterals were stimulated in the *stratum oriens*, while compound EPSPs were recorded in CA3 pyramidal neurons in the whole-cell current-clamp recording configuration. Compound excitatory postsynaptic potentials (EPSPs) were isolated in presence of 10 µM gabazine (Fig. 11a). EPSPs

evoked by presynaptic axons stimulation showed an average peak amplitude of 2.0 ± 0.3 mV, which suggests that compound synaptic signals were on average comprised of ~5 unitary synaptic events (Fig. 11b; Guzman et al., 2014b). An average latency of 2.9 ± 0.5 ms suggest that compound EPSPs were monosynaptic (Fig. 11c). The average 20 – 80% rise time of 5.0 ± 0.2 ms, and decay time constant of 107.0 ± 5.0 ms explains the distantly located synapses and summation of synaptic events respectively (Fig. 11d, e). These parameters are consistent with previously reported properties of CA3–CA3 EPSPs (Zalutsky and Nicoll, 1990).

We then examined the contribution of NMDAR channels since they are involved in most forms of plasticity. We added D-AP5 (an antagonist of NMDARs; 20 µM) to the bath solution and measured the difference in EPSP peak amplitude and its voltage-time integral before and during D-AP5. The postsynaptic neuron was loaded with QX-314 (5 mM) to block EPSP amplification by voltage-activated channels. Compound EPSPs were measured at different membrane potentials. At –70 mV, a difference between the EPSPs was not detectable (Fig. 11f, g) whereas at –20 mV, both peak amplitude and the voltage-time integral were substantially reduced. The component blocked by D-AP5 probably reflects the contribution of NMDA-type glutamate receptors.

Further, we tested if the stimulation of C/A synapses was selective without any contamination from mossy fiber inputs to CA3. Bath application of 1 µM DCG-4 (a group II mGluR agonist), which is expected to block contaminating mossy fiber inputs (Kamiya et al., 1996) has no significant effect on the compound EPSPs (Fig. 11h). Cells in which DCG-4 inhibited the compound EPSP amplitude by more than 15% were excluded from further analysis.

3.2 Synaptic Plasticity by high-frequency stimulation

To examine whether synaptic responses of CA3–CA3 recurrent collaterals are able to undergo plastic changes, we first tested a standard HFS induction protocol, a paradigm expected to maximally potentiate synapses (Zalutsky and Nicoll, 1990). Four trains of 100 presynaptic stimuli at 100 Hz for one second repeated every 10 seconds were applied to presynaptic axons. HFS resulted in

a marked long-lasting potentiation of EPSP peak amplitude (Fig. 12a, b). On average, the amount of potentiation 20−30 min after the induction protocol was 201 ± 21% (range: 253 – -4 %; 12 cells, P<0.01; Fig. 12b).

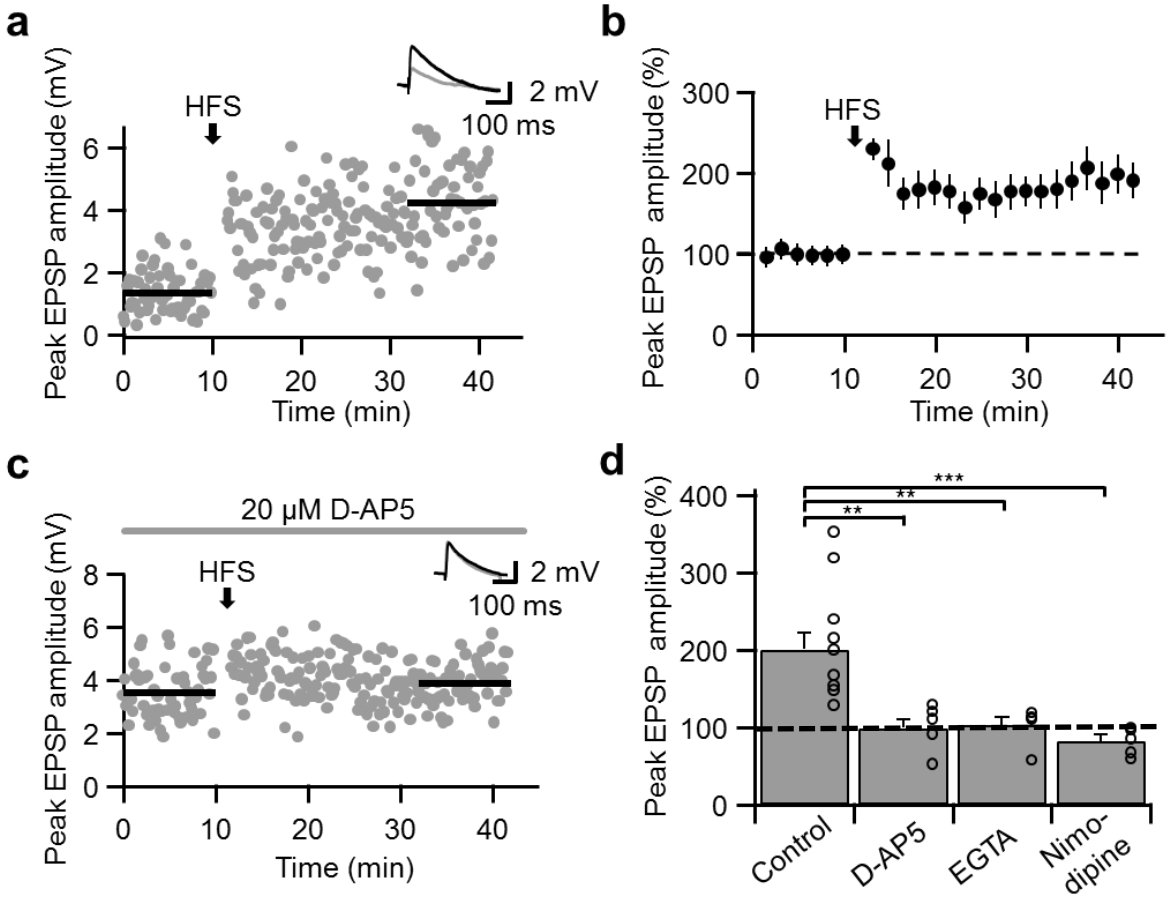

Figure 12: HFS induced LTP at CA3–CA3 recurrent synapses

(a) Plot of compound EPSP peak amplitude against experimental time before and after application of HFS (arrow) in a single experiment. Inset shows the average of 60 EPSP responses before (gray) and 30 min after HFS (black).
(b) Plot of average compound EPSP peak amplitude against experimental time before and after application of HFS (arrow) in 12 experiments (P = 0.0002). EPSP amplitude was normalized to the control value before HFS (dashed line).
(c) Bath application of 20 µM the NMDAR antagonist D-AP5 prevented the increase of EPSP amplitude after HFS, showing that HFS-induced LTP induction required the activation of NMDARs. Single representative experiment.
(d) Summary bar graph showing the effect of extracellular D-AP (20 µM; 6 cells), intracellular EGTA (20 mM; 5 cells), and extracellular nimodipine (10 µM; 5 cells). Note that antagonists of NMDARs, Ca^{2+} chelators, and blockers of voltage-gated Ca^{2+} channels all inhibit HFS-induced LTP.

LTP induction by HFS is generally NMDAR-dependent (Bliss and Collingridge, 1993; Malenka and Nicoll, 1999). NMDAR blocker D-AP5 (20 µM) completely abolished HFS-induced potentiation (99 ± 11%; 6 cells; P = 0.001; Fig. 12c, d) suggesting LTP to be NMDAR-dependent.

It is well established that activation of NMDARs during LTP induction leads to an influx of Ca^{2+} within the dendritic spine, a chemical process critical to LTP induction (Lynch et al., 1983; Malenka et al., 1988, 1992). To test the Ca^{2+} dependence of LTP induction, the postsynaptic cell was dialyzed with slow Ca^{2+} chelator EGTA (Hoffman et al., 2002; Fig. 12d). 20 mM EGTA completely abolished HFS-induced LTP (102 ± 11%; 5 cells; P = 0.003). These results show that a rise in postsynaptic Ca^{2+} concentration is necessary for LTP induction. Furthermore, since EGTA has slow Ca^{2+}-binding kinetics, the results indicate that Ca^{2+} source (i.e. NMDAR) and Ca^{2+} sensor are relatively far away.

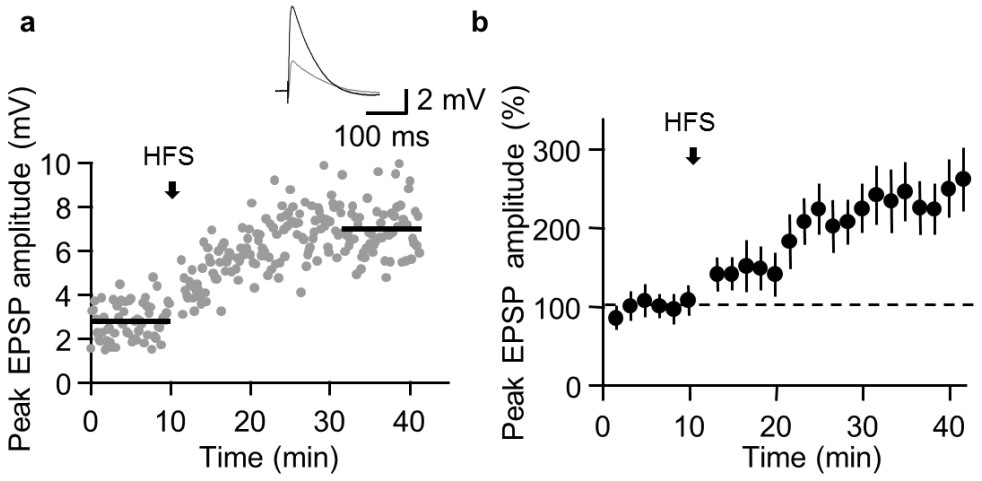

Figure 13: HFS induced LTP at near physiological temperature

(a) EPSP peak amplitude against experimental time before and after application of HFS (arrow) in a single experiment at ~33°C. Inset shows the average of 60 EPSP responses before (gray) and 30 min after HFS (black).
(b) Normalized EPSP peak amplitude against experimental time before and after application of HFS (arrow) in 12 experiments (P = 0.002).

It has been shown at Schaffer collateral (CA3)–CA1 synapses that LTP induction requires Ca^{2+} influx through either NMDARs or postsynaptic voltage gated Ca^{2+} channels (Grover and Teyler, 1990). To test whether LTP induction

at CA3–CA3 synapses also requires two independent Ca^{2+} sources, we examined the effect of L-type Ca^{2+} channel blocker on the potentiation. In the presence of 10 µM nimodipine, the extent of potentiation was 82 ± 8% (5 cells; P = 0.0007; Fig. 12d) suggesting a role of L-type Ca^{2+} channels in the LTP induction.

The enzymatic machinery responsible for potentiation may function differently at physiological temperature. We tested whether LTP can be induced at near physiological temperature (~33° C). The magnitude of potentiation was 240 ± 21% (6 cells, P=0.002; Fig.13).

In summary HFS induces robust potentiation at CA3–CA3 recurrent synapses which requires influx of Ca^{2+} through at least two sources NMDARs and L-type Ca^{2+} channels (Table 1).

3.3 Role of Na^{+} channels for HFS induced LTP

We next examined whether postsynaptic spiking is necessary for induction of LTP by HFS. We divided our HFS data into two subsets. In the first subset we had cells where we observed postsynaptic spiking during HFS. No postsynaptic spiking was observed during HFS in the second subset (Fig. 14a).

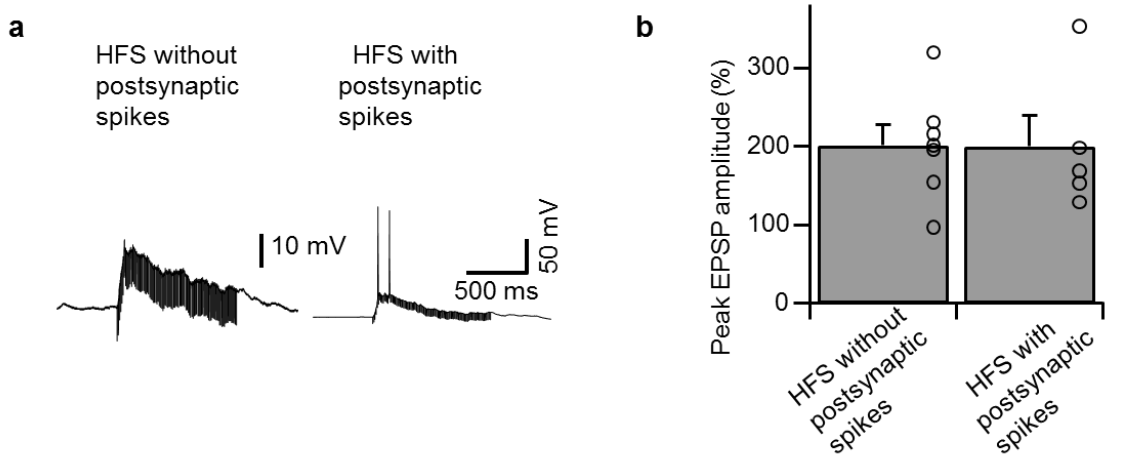

Figure 14: Axosomatic spikes are not required for HFS induced LTP

(a) Voltage deflection during HFS. Note on the left HFS without any axosomatic spikes.
(b) Summary bar graph shows LTP amplitude in both the conditions (HFS without spikes and HFS with spikes).

We analyzed the magnitude of potentiation between these two subsets. Interestingly, the extent of LTP was 200.0 ± 39.8 % in the first subset (HFS with postsynaptic spiking) and 201.6 ± 26 % in the second subset (HFS without postsynaptic spiking). There was no significant difference between the two groups (5 and 7 cells, respectively, P = 0.64; Fig. 14b). Thus, the induction of LTP by HFS at CA3–CA3 recurrent synapses did not require axosomatic spiking in the postsynaptic cell. An alternative to the axosomatic spike would be local dendritic spikes which might play a role in induction of LTP (Kim et al., 2015).

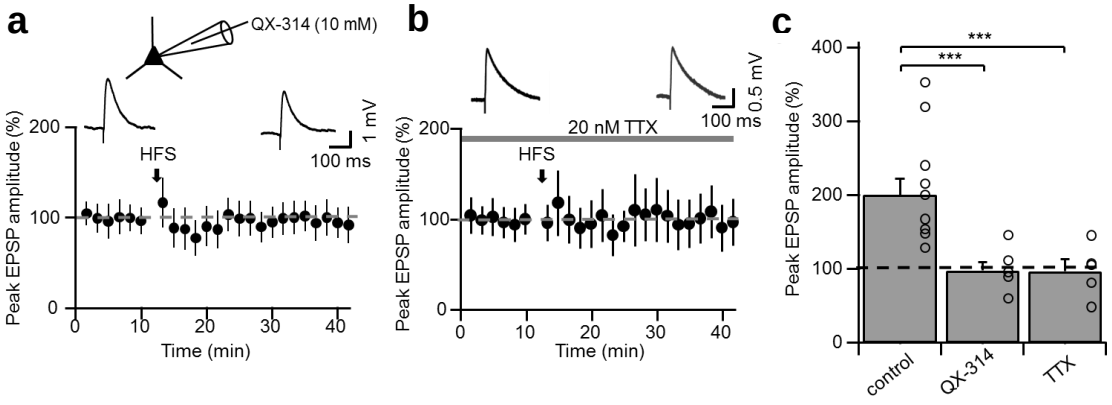

Figure 15: HFS- induced LTP at CA3–CA3 synapses requires Na^+ channels

(a) Schematic of recording configuration where postsynaptic cell was dialyzed with QX-314 (10 mM) intracellularly. Plot of average compound EPSP peak amplitude against experimental time before and after HFS in the presence of intracellular QX-314 (6 cells; P = 0.008). Intracellular application of QX-314 completely abolishes LTP.
(c) Bath application of TTX (20 nM) also blocked LTP induction by HFS. Red line at the bottom shows the application of TTX (20 nM; 5 cells; P = 0.002).
(d) Summary bar graph showing the effect of intracellular QX-314 (10 mM; 6 cells, P = 0.008) and bath application of TTX (20 nM; 5 cells, P = 0.002) against control experiments. Both Na^+ channel blockers completely abolish LTP suggesting that local active processes (e.g. dendritic Na^+ spikes) may contribute to potentiation.

These results appear to be consistent with the hypothesis that dendritic spikes, which occur prominently in the apical dendrites of CA3 pyramidal neurons (Kim et al., 2012), play an important role in LTP following the HFS induction protocol. To test the hypothesis that passive synaptic depolarization is enough for LTP

induction, we employed different Na^+ channel blockers (QX-314 and low concentration of TTX). We dialyzed the postsynaptic cell with 10 mM QX-314 and applied the HFS for LTP induction. Significant reduction in magnitude of LTP from 201 ± 21 % under drug-free conditions to 98 ± 12 % was observed (6 cells; P = 0.008; Figure 15 a, c). In another set of experiments, bath application of low concentration of TTX (20 nM), which otherwise has no presynaptic effect; Kim et al., 2015), also abolished LTP induction by HFS (98 ± 16 %; 5 cells; P = 0.002; Figure 15 b, c).

These results indicate the role of Na^+ channels in the induction of LTP. Therefore, we can conclude that in the absence of axosomatic spikes, dendritic spikes may contribute to the depolarization needed for Ca^{2+} entry through NMDARs.

HFS is the most conventional protocol to induce LTP. However, it does not explain the temporal correlation between EPSP and postsynaptic AP. Postsynaptic AP propagates back very effectively into the dendritic tree in CA3 pyramidal neurons (Kim et al., 2012) and thus would act as an associative signal for LTP induction (Stuart and Sakmann, 1994). An associative protocol, e.g. pairing presynaptic stimulation/spikes with postsynaptic AP/APs at low frequency, may provide the critical requirement of temporal correlation between presynaptic and postsynaptic activity (Markram et al., 1997; Magee and Johnston, 1997; Bi and Poo, 1998; Zhang et al., 1998; Sjöström et al., 2001; Feldman, 2012). Therefore, we studied the spike timing-dependent plasticity by pairing single EPSP with a postsynaptic AP.

3.4 Spike timing-dependent plasticity rule at CA3–CA3 synapses

Timing of spikes to synaptic input has a strong effect on synaptic strength (Magee and Johnston, 1997; Markram et al. 1997; Bi and Poo, 1998). In Hebbian STDP the order and time interval between presynaptic activity (EPSPs / APs) and postsynaptic spikes determine the sign and magnitude of plasticity. A pre–postsynaptic sequence of activity leads to LTP whereas a post–presynaptic sequence results in LTD. Although STDP has been demonstrated in CA3 neurons in organotypic slice culture (Debanne et al.,

1997; Montgomery et al., 2001), its properties in acute hippocampal preparations have remained unclear.

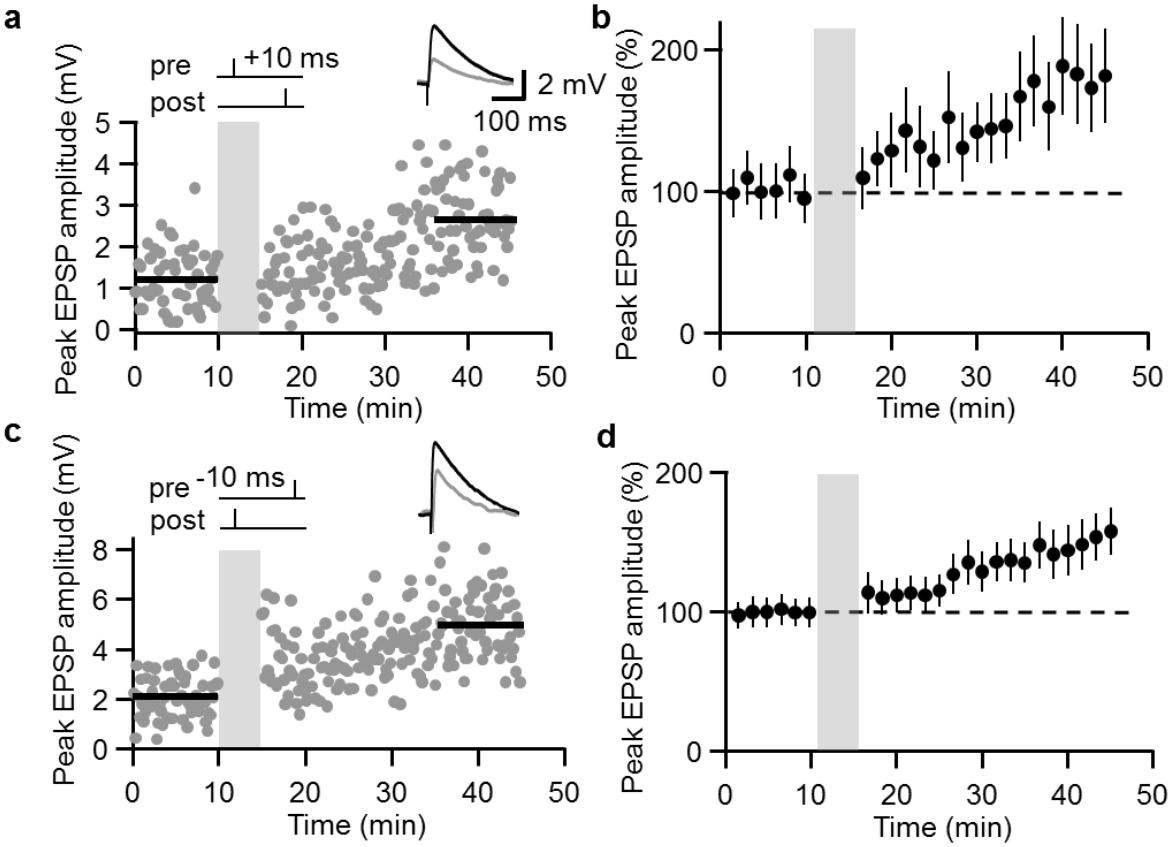

Figure 16: STDP induction rules at CA3–CA3 recurrent synapses

(a, b) Plot of compound EPSP peak amplitude against experimental time before and after pre–postsynaptic pairing (Δt=+10 ms). Single-cell data (a) and mean data (b; 9 cells; P = 0.004).
(c, d) Similar plot as in (a, b), but for post–presynaptic pairing (with Δt=–10 ms). Single-cell data (c) and mean data (d; 15 cells; P = 0.0004). Insets in a and c show the average of 60 evoked EPSPs before (black) and 20–30 min after induction (gray). In b and d, EPSP amplitude was normalized to the control value before LTP induction (dashed line). Gray vertical bars indicate the time intervals in which the induction paradigms were applied.

Therefore, we tested the effects of a pairing paradigm, in which presynaptic stimulation (EPSP) and postsynaptic AP were paired at different time intervals (Fig. 16 and 17). We first tested the effects of a pairing paradigm in which single EPSP was followed by a postsynaptic current pulse at a 10-ms interval (i.e. a pre–postsynaptic sequence). This pairing protocol, repeated 300 times at a frequency of 1 Hz, induced a robust LTP (178.0 ± 22.1%, 9 cells; P = 0.004;

Fig. 16a, b; Table 1). LTP was associative, since neither EPSPs nor postsynaptic APs induced LTP when presented in isolation (isolated presynaptic stimulation: 107.9 ± 5.6%, 5 cells, P = 0.19; isolated postsynaptic stimulation: 92.9 ± 7.9%; 5 cells, P = 0.44; Fig. 18). Thus, CA3–CA3 recurrent synapses exhibited an associative form of LTP, with an extent of potentiation comparable to that of HFS induced LTP.

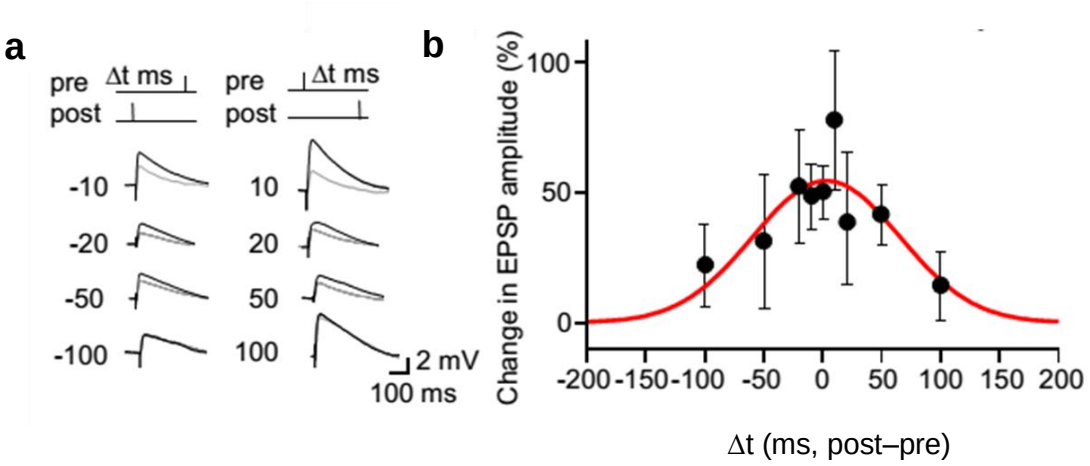

Figure 17: STDP magnitude for different EPSP–AP time intervals (Δt)

(a) Representative average traces (gray, before induction; black, 20–30 min after induction),
(b) Plot of LTP magnitude (expressed as % increase over baseline) against Δt.
Red curve, Gaussian function fit to the data points. Note that the STDP window was broad and largely symmetric.
Thus, timing of pre- and postsynaptic activity, but not its temporal order, determines the magnitude of STDP at CA3–CA3 synapses.

Next, we tested pairing protocols with an inverse (i.e. post–presynaptic) sequence stimulation where postsynaptic AP was followed by EPSP at 10 ms time interval (Fig. 16c). Such a pairing protocol led to an increase of EPSP amplitude, to 148.0 ± 12.0% of the control value (15 cells; P = 0.0004; Fig. 16c, d).

Since the order of pairing (pre–postsynaptic or post–presynaptic) at close time interval (10 ms) does not have any effect on the sign of plasticity and always led to LTP, we tested pairing protocols with different time intervals between pre- and postsynaptic stimulation (Fig. 17a, b). Plotting the magnitude of LTP

against pairing time interval ∆t revealed that the STDP induction curve was nearly symmetric and broad, with a maximum near ∆t = 0 and a half-duration of 147 ms (Fig. 17b). Similar results were obtained at near-physiological temperature (~33°C); the maximal amount of LTP and the shape of the curve were comparable with only minimal variation in the half-width (133 ms; Fig. 20).

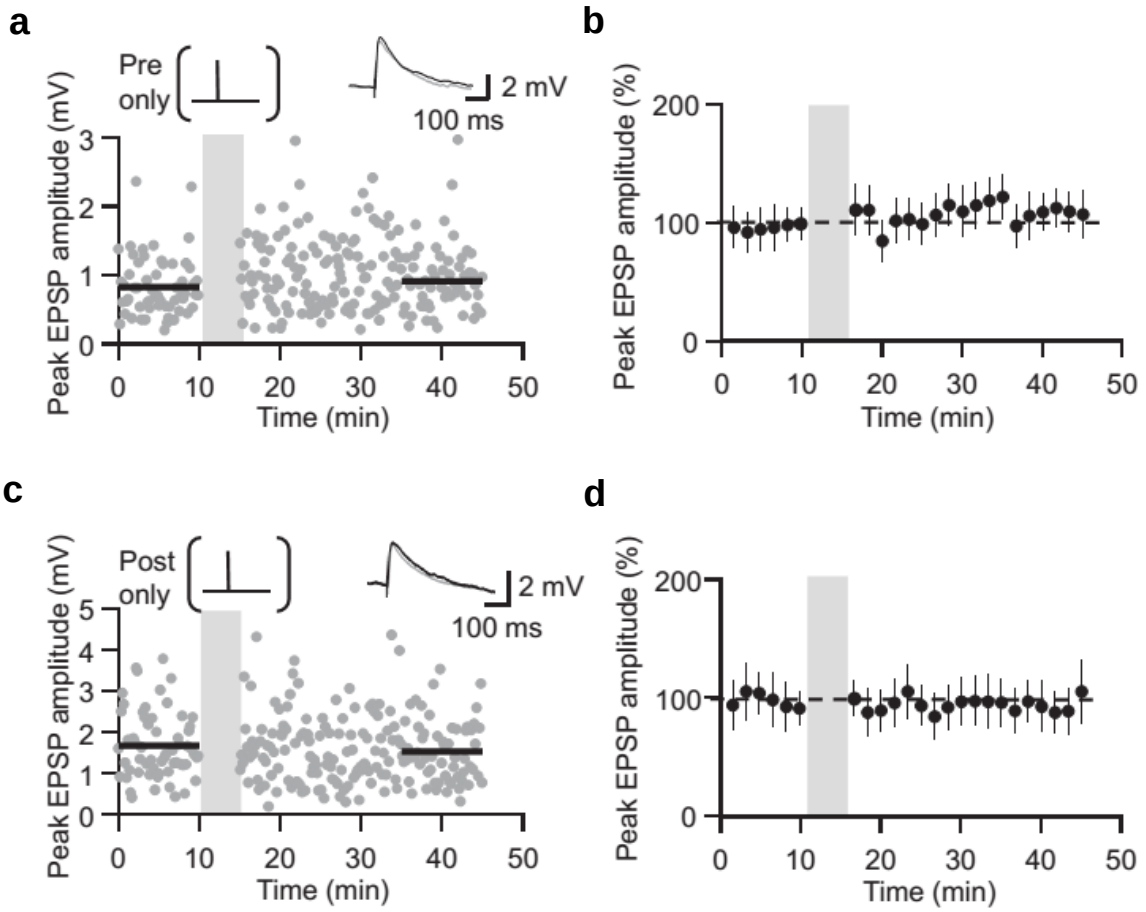

Figure 18: Pairing-induced LTP at CA3–CA3 synapses is associative

(a, b) Plot of average compound EPSP peak amplitude against experimental time before and after application of isolated presynaptic stimulation. Data from a single representative experiment (a) and mean from 5 experiments (b; P = 0.19).
(c, d) Similar plot, before and after isolated postsynaptic stimulation. Data from a single representative experiment (c) and mean from 5 experiments (d; P = 0.44).
Insets in a and c show the average of 60 evoked EPSPs before (gray) and 30 min after paradigm application (black). Gray vertical bars indicate the time intervals in which the induction paradigms were applied.

3.5 Mechanism of spike timing-dependent LTP at CA3–CA3 synapses

Next, we compared the mechanisms of spike timing-dependent LTP induced by pre–postsynaptic versus post–presynaptic sequences. Pairing-induced LTP was abolished by bath-application of 20 µM D-AP5 (101.2 ± 5.2%, 7 cells; P = 0.034; Fig. 19a for pre–postsynaptic sequence and (100.5 ± 4.2%, 6 cells, P = 0.006, Fig. 19b for the post– presynaptic sequence). Thus, NMDAR activation was necessary for LTP induction.

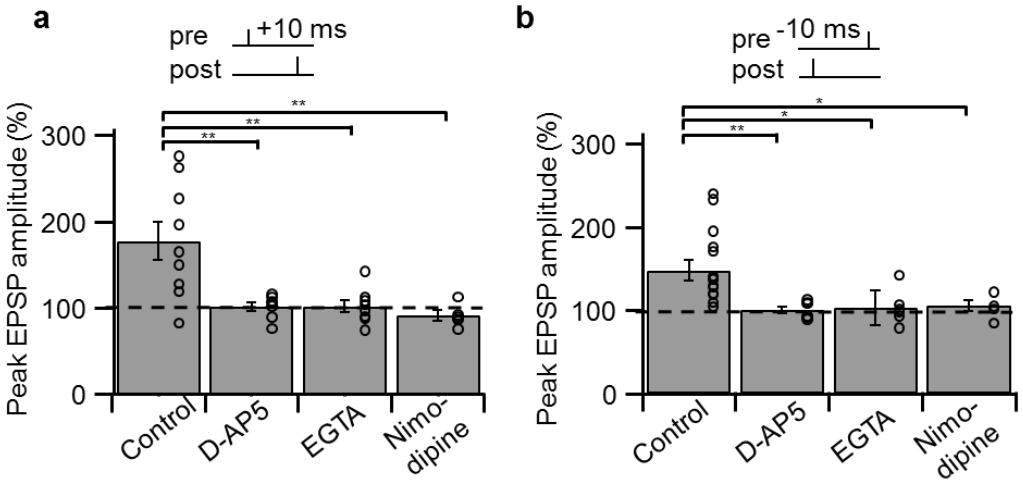

Figure 19: Pharmacology of STDP at CA3–CA3 synapses

(a, b) Summary bar graph showing the effects of 20 µM extracellular D-AP5, 20 mM intracellular EGTA (8 and 5 cells), and 10 µM extracellular nimodipine (5 and 5 cells, respectively) on pairing-induced LTP for pre–postsynaptic (a) and post–presynaptic sequences (b) Circles represent data from individual cells, bars indicate mean ± S.E.M. LTP with both pairing paradigms was largely abolished by all manipulations, demonstrating that multiple Ca^{2+} sources are necessary for LTP induction.

Furthermore, pairing-induced LTP was abolished by dialyzing postsynaptic cell with 20 mM Ca^{2+} chelator EGTA (101.8 ± 7.2%, 8 cells; P = 0.007; Fig. 19a for the pre–postsynaptic sequence and 103.0 ± 21.0%, 5 cells, P = 0.018, Fig. 19b for the post–presynaptic sequence). Thus, a rise in postsynaptic Ca^{2+} concentration was necessary for LTP induction.

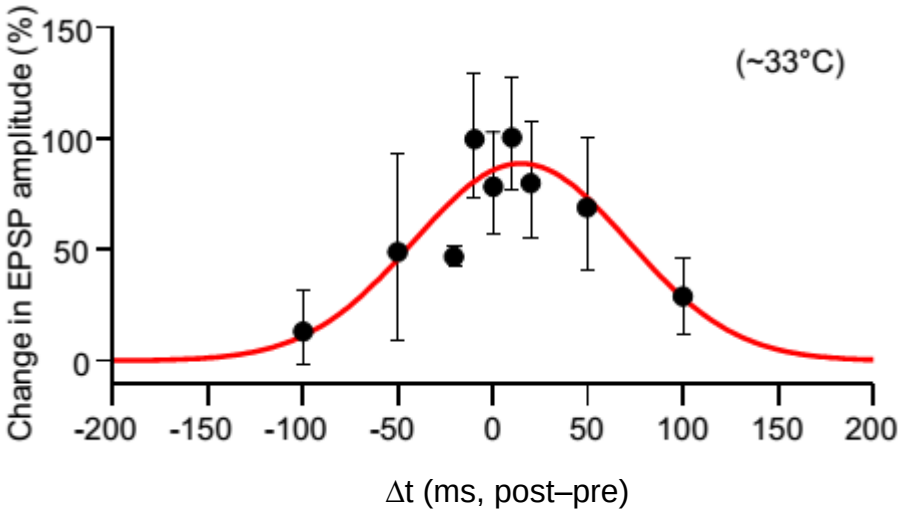

Figure 20: STDP in CA3–CA3 synapses at near-physiological temperature

Plot of STDP magnitude (expressed as % increase over baseline) against time interval of pairing between EPSP and AP (Δt) at near-physiological temperature (~33°C). Red curve, Gaussian function fit to the data points. Note that the STDP curve was broad and symmetric, similar to the STDP curve at room temperature (Fig. 17b).

Finally, similar to HFS induced potentiation, pairing-induced LTP was also inhibited by bath application of 10 µM nimodipine (91.1 ± 6.0%, 5 cells; P = 0.011; Figure 19a for the pre–postsynaptic sequence and 105.0 ± 6.1%, 5 cells, P = 0.019, Figure 19b for the post–presynaptic sequence). Thus, an elevation of postsynaptic Ca^{2+} through activation of either NMDARs or L-type Ca^{2+} channels was necessary for LTP induction by both pre–postsynaptic and post–presynaptic pairing (Table 1).

In conclusion, CA3–CA3 recurrent synapses exhibited robust spike timing-dependent potentiation, the magnitude of which varies strongly with the pairing time interval. Thus, the STDP induction rule at CA3–CA3 recurrent synapses was unique, differing from previously reported STDP rules for glutamatergic synapses in a variety of circuits (Feldman, 2012).

3.6 Potentiation at single synapses

An increase in postsynaptic Ca^{2+} concentration is required for LTP of glutamatergic synapses (Bliss and Collingridge, 1993). This increase in Ca^{2+} concentration may be restricted to a single spine (Denk et al., 1995; Yuste and Denk, 1995). Since we know from our electrophysiology data that spike timing-

dependent LTP at CA3–CA3 recurrent synapses depended on an increase in postsynaptic Ca^{2+} presumably in dendritic spines (Koester and Sakmann, 1998; Nevian and Sakmann, 2006), we measured [Ca^{2+}] dynamics at a single spine. We employed confocal microscopy to measure summation of [Ca^{2+}] transients on pairing time intervals of EPSP and AP in single spines of CA3 pyramidal neurons (Fig. 21, 22, 23).

3.6.1 Properties of spine [Ca^{2+}] transients

Reactive dendritic spines were located 50–200 µm from the soma. [Ca^{2+}] transients were evoked either by EPSPs following stimulation of nearby CA3 cell axons, or by bAPs following somatic current pulses (Fig. 21a, b). We first examined the pharmacological properties of [Ca^{2+}] transients. High-frequency AP waveform (5 APs at 100 Hz) revealed that the Ca^{2+} indicator Fluo-5F was not saturated under our experimental conditions (Fig. 22a). Synaptic stimulation and bAPs evoked [Ca^{2+}] transients with comparable amplitude, but different spatial profiles (Fig. 21b). [Ca^{2+}] transients evoked by synaptic stimulation were larger in the spine than in the adjacent shaft, whereas transients evoked by bAPs showed similar amplitudes in the two locations (Fig. 21b). [Ca^{2+}] transients evoked by synaptic stimulation were enhanced by removal of Mg^{2+} from the bath solution and blocked by 20 µM CNQX and 20 µM D-AP5, suggesting a contribution of NMDA-type glutamate receptors (Fig. 22c, d). [Ca^{2+}] transients evoked by bAPs were completely blocked by 200 µM Cd^{2+} or 10 µM nimodipine, indicating that they were generated by Ca^{2+} inflow through voltage-gated Ca^{2+} channels (Fig. 22b).

We next examined the effect of the pairing protocol that induced spike timing-dependent LTP on single spine [Ca^{2+}] transients. Pairing of EPSPs and bAPs with short time intervals (Δt either +10 ms or –10 ms) substantially enhanced the amplitude of the [Ca^{2+}] transients (Fig. 23a). Using the peak amplitude for quantification, [Ca^{2+}] transients evoked by pre–postsynaptic sequences (i.e. Δt = +10 ms) were 2.96 ± 0.87-fold larger than those by EPSPs alone (Fig. 23b).

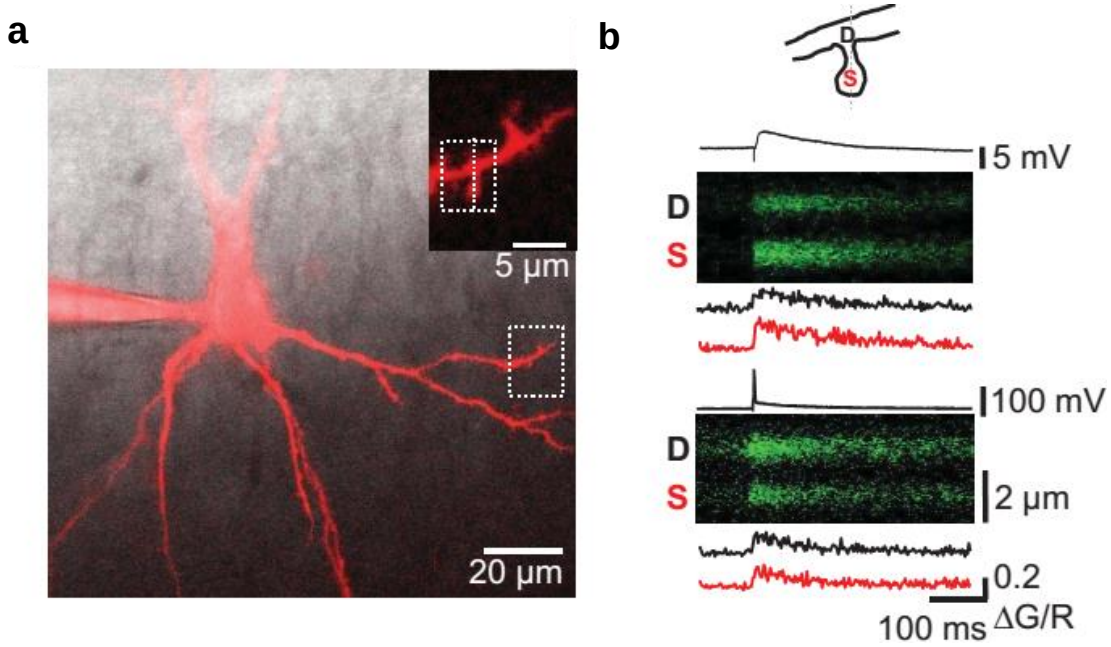

Figure 21: EPSP- and AP-induced [Ca^{2+}] transients in spines of CA3 neurons

(a) Fluorescence image of a CA3 pyramidal neuron loaded with Fluo-5F and Alexa Fluor 594 (maximum projection of stack of 48 1-µm confocal sections; excitation wavelength 594 nm). The region indicated by the box is shown on an expanded scale in inset.
(b) Spine [Ca^{2+}] transients evoked by synaptic stimulation and bAPs. Top, schematic illustration of the line scan configuration (dotted line, 400 Hz). Center, [Ca^{2+}] transient during a synaptically evoked EPSP. Bottom, [Ca^{2+}] transient during a bAP.
In each panel, upper graph represents membrane potential trace, middle shows G fluorescence signal against distance (vertical axis) and time (horizontal axis), and bottom indicates $\Delta G / R$ versus time in the dendrite (black) and the spine (red).

Similarly, [Ca^{2+}] transients evoked by post–presynaptic sequences (i.e. Δt = –10 ms) were 2.80 ± 0.86-fold larger than those by isolated EPSPs (6 cells; Fig. 23b). Similar results were obtained using the area under the [Ca^{2+}] transients for quantification (Fig. 23c). [Ca^{2+}] transients evoked by combined stimulation were significantly larger than the arithmetic sum of [Ca^{2+}] transients evoked by APs or EPSPs in isolation. On average, the degree of nonlinearity was 131.1 ± 6.0% for Δt = +10 ms and 132.9 ± 4.3% for Δt = –10 ms (P = 0.002 in both cases; Fig. 23d).

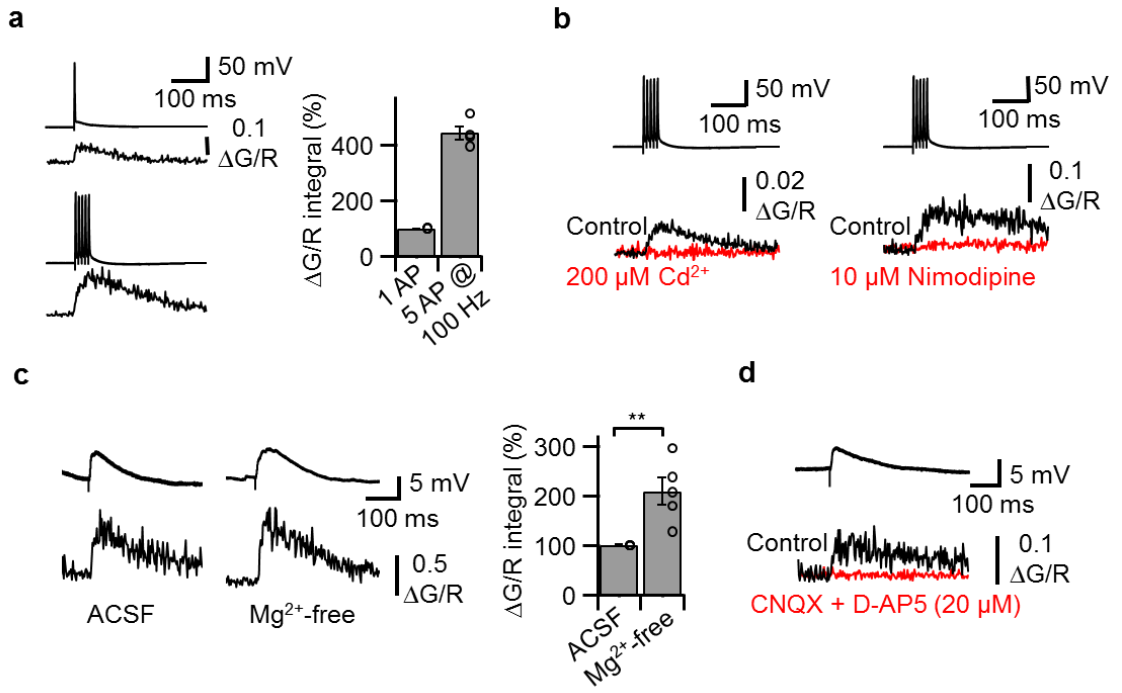

Figure 22: Pharmacological properties of spine and dendritic [Ca^{2+}] transients

(a) Dendritic [Ca^{2+}] transients evoked by a single AP and a 100-Hz train of APs. Left, Average [Ca^{2+}] transients. Right, summary bar graph of normalized peak amplitudes.
(b) Dendritic [Ca^{2+}] transients evoked by backpropagated APs are blocked by 200 μM Cd^{2+} (left) or 10 μM of the L-type Ca^{2+} channel blocker nimodipine (right). Black traces, control; red traces, in the presence of blocker.
(c) Spine [Ca^{2+}] transients evoked by synaptic stimulation are increased in Mg^{2+}-free extracellular solution. Left, [Ca^{2+}] transients in standard ACSF; right, [Ca^{2+}] transients in Mg^{2+}-free solution. Right, summary bar graph of normalized [Ca^{2+}] transient integrals in the two conditions.
(d) Spine [Ca^{2+}] transients evoked by synaptic stimulation are blocked by 20 μM CNQX + 20 μM D-AP5. Black traces, control; red trace, in the presence of blockers.

Thus, pairing of EPSPs and APs led to a supralinear response in the spine [Ca^{2+}] transients, explaining the associative nature of STDP (Fig. 16).

We next measured the amount of summation at different pairing time intervals between EPSP and postsynaptic AP (Fig. 24a). The amplitude of the spine [Ca^{2+}] transients were smaller at longer time intervals, which explains the lack of potentiation found in our electrophysiology data. A plot of spine [Ca^{2+}] transient against pairing time interval Δt revealed a symmetric and broad summation curve (Fig. 24a). The half-duration of the summation curve was 81 ms, comparable to the STDP induction curve (Fig. 17b).

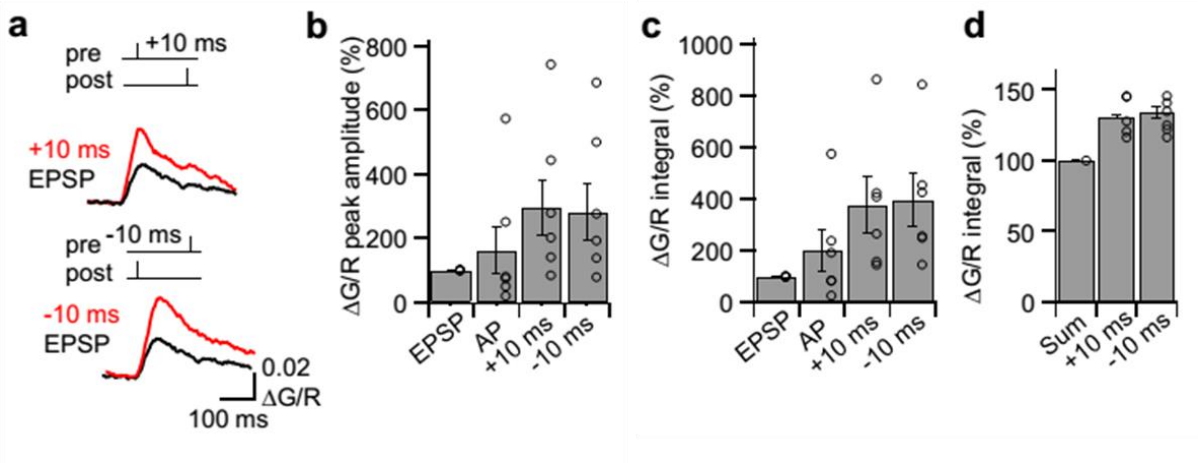

Figure 23: Summation of EPSP- and AP-induced [Ca^{2+}] transients in CA3 spines

(a) [Ca^{2+}] transients during EPSPs (black traces), pre–postsynaptic pairing (Δt = +10 ms; red trace, top), and post–presynaptic pairing (Δt = –10 ms; red trace, bottom). Note that pairing markedly increased the peak amplitude of the [Ca^{2+}] transient in comparison to isolated EPSPs.
(b, c) Summary of the amplitude (b) and integral (c) of [Ca^{2+}] transients evoked by single EPSPs, single APs, pre–postsynaptic pairing (Δt = +10 ms), and post–presynaptic pairing (Δt = –10 ms). Data were normalized to the EPSP value. Circles represent data from individual cells, bars indicate mean ± S.E.M.
(d) Summary of integral values, normalized to the arithmetic sum of EPSP and AP values. Note supralinearity of summation.

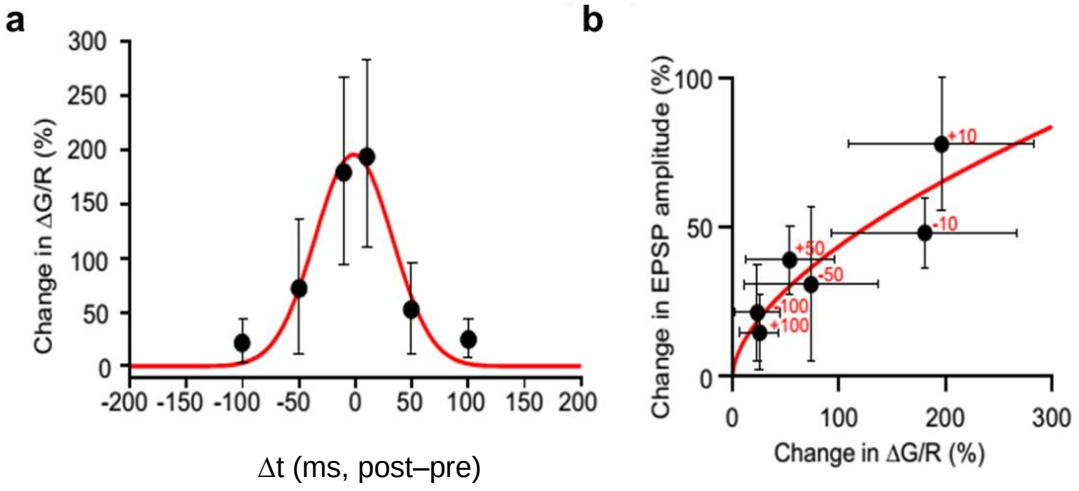

Figure 24: Time-dependence of summation of [Ca^{2+}] transients in CA3 spines

(a) Peak amplitude of [Ca^{2+}] transients during combined pre–postsynaptic or post–presynaptic stimulation, normalized to that of isolated EPSPs, plotted against pairing time interval Δt. Red curve, Gaussian function fit to the data points. Note that the [Ca^{2+}] transient amplitude versus pairing interval curve was broad and symmetric, similar to the STDP curve.
(b) Plot of change in EPSP amplitude against change of [Ca^{2+}] transients during different pairing sequences. Numbers near symbols represent the values of Δt between AP and EPSP (red, in ms). EPSP potentiation data were taken from Fig. 17.

To further quantify the relation between the peak amplitude of [Ca^{2+}] transients and the extent of potentiation, we plotted the two parameters against each other for all Δt values and fit the data with a power function (Fig. 24b). This analysis revealed a monotonically rising relation between potentiation and [Ca^{2+}] transients, irrespective of the order of APs and EPSPs.

Thus, temporally symmetric summation of the [Ca^{2+}] transients in dendritic spines appears to be the mechanism underlying the temporal symmetry of STDP induction in CA3–CA3 recurrent synapses.

3.7 A CA3 network model with a symmetrical STDP rule

What are the implications of noncanonical STDP induction rules for the memory function of the CA3 network? To address this question, we simulated storage and recall in a network model of pattern completion (Fig. 25 and 26) based on previous models (Marr, 1971; Hopfield, 1982; Gibson and Robinson, 1992; Bennett et al., 1994; Fig. 25a), but additionally incorporated the time dependence of both spiking and plasticity. 3000 neurons were connected by excitatory synapses. Excitatory synapses were endowed with either symmetric (this study) or asymmetric plasticity rules (Bi and Poo, 1998; Fig. 25b). In the storage phase, a defined test pattern with temporal spread of activity was applied to the first 300 cells (corresponding to an activity of 0.1). Subsequently, several additional random patterns were applied, leading to potentiation of synapses in the synaptic matrix (Fig. 25c). In the recall phase, an incomplete test pattern was applied (Fig. 25d). For perfect recall, the original test pattern (i.e. the first 300 cells) should be selectively reactivated after a number of recall cycles. By contrast, for impaired recall, the number of valid firings would be reduced, while the number of spurious firings is expected to increase. Finally, we quantified the quality of recall as the correlation between original patterns and retrieved patterns, and capacity of the network as the maximal number of patterns that could be loaded without recall impairment (Methods; Table 2).

When our new plasticity rule was implemented, the recall of the original patterns was robust, and the capacity of the network was 58.1 patterns (Fig. 26a). In contrast, when an asymmetric LTP induction rule (Bi and Poo, 1998)

was incorporated, the recall of the pattern was markedly impaired (capacity 4.5 patterns; Fig. 26b).

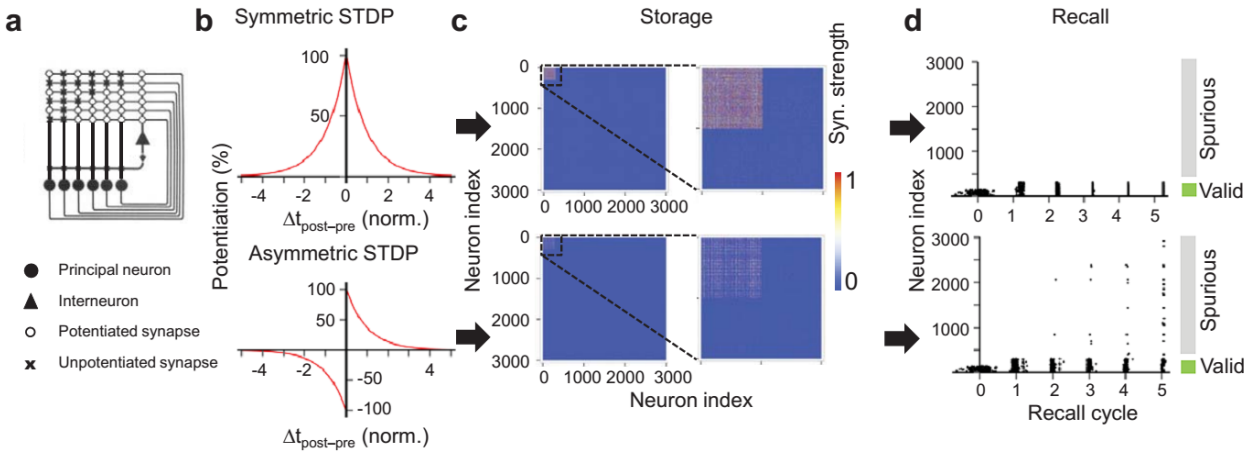

Figure 25: An autoassociative network model of pattern completion

(a) Schematic illustration of network topology. The model is composed of several principal neurons (large filled circles) and a single inhibitory interneuron (large filled triangle). Principal cells are interconnected by excitatory synapses (potentiated, small open circles; unpotentiated, small crosses). In the schematic shown, there are six pyramidal cells; the real model was composed of 3,000 pyramidal neurons. The mixture of potentiated and unpotentiated synapses in the matrix was generated by prior application of three binary activity patterns (001011, 101010, and 000111). Modified from McNaughton and Morris, 1987.

(b) Plasticity rules. Top, symmetric plasticity rule, as supported by the present results for CA3–CA3 synapses. Bottom, asymmetric plasticity rule, as reported in other studies (Bi and Poo, 1998; Magee and Johnston, 1997; Markram et al., 1997). Δt was given in normalized units, which could correspond to one theta oscillation cycle (~200 ms). For details, see Methods.

(c) Storage of patterns in the synaptic matrix. Synaptic strength was represented as temperature map (red, maximal potentiation; blue, unpotentiated). A single test pattern in the first 300 neurons and 10 additional patterns in randomly selected neurons were applied during storage, with randomized spike time in both cases. Ordinate is index of presynaptic neuron; abscissa is index of postsynaptic neuron. Insets (right) show expanded views of the matrix for first 600 cells. Note that the symmetric plasticity rule (top) induces a higher average potentiation than the asymmetric rule (bottom).

(d) Recall of patterns in the network model. Recall was triggered by the partial test pattern (50% valid firings, no spurious firings in comparison to the original pattern) with randomized spike timing. With the symmetric plasticity rule (top; g_1 = 0.3), the original pattern was perfectly retrieved after three recall cycles. In contrast, with the asymmetric plasticity rule (bottom; g_1 = 0.1), retrieval was only partial, with a decrease in the number of valid firings and an increase in the number of spurious firings.

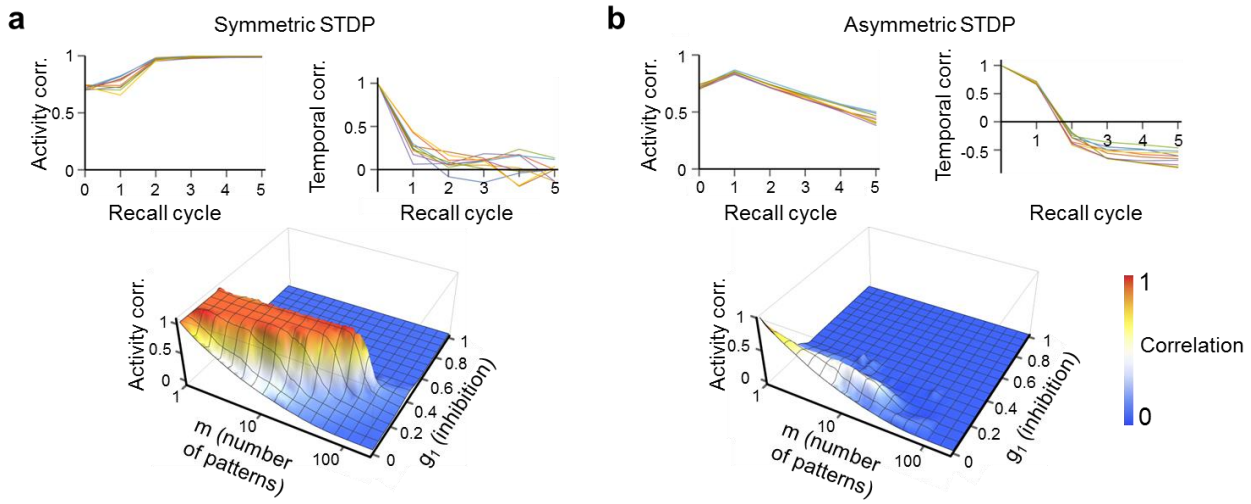

Figure 26: Robust recall of original patterns with asymmetric STDP rule

(a, b) Top, differential dependence of activity correlation (left) and spike-time correlation for active cells (right) for symmetric and asymmetric STDP rules on recall cycle number. Lines with different colors represent the pattern correlation trajectories for 10 patterns. For the symmetric STDP rule, activity correlation increases, whereas spike-time correlation is eliminated. For the asymmetric STDP rule, activity correlation declines, whereas spike-time correlation becomes inverted. Bottom, 3D-plot of activity correlation at the 5th recall cycle versus pattern load m and the proportionality factor g_1 of inhibition for the symmetric (a) and the asymmetric (b) plasticity rule. For the symmetric plasticity rule, the capacity was 58.1, whereas for the asymmetric rule it was only 4.5.

Thus, in our model, the symmetric STDP induction rule facilitated the storage and recall of information by incomplete input, conveying the ability of pattern completion. Remarkably, the symmetric STDP rule led to only minimal temporal correlation between spike times in the original patterns and the retrieved patterns, because synchronization of activity emerged during the recall phase(Fig. 26a, top right). In contrast, the asymmetric STDP rule generated a significant negative temporal correlation between original and retrieved patterns after the first five recall cycles (Fig. 26b, top right). Thus, the symmetric STDP rule is advantageous for pattern completion, whereas asymmetric rules may be superior for the storage and recall of temporal AP sequences, e.g. during spatial learning (Abbott and Blum, 1996).

Table 1: Synaptic plasticity at CA3–CA3 recurrent synapses

Basic properties of compound EPSPs at hippocampal CA3–CA3 cell synapses

Property (n = 17)	Value
Peak EPSP (mV)	2.0 ± 0.3
Latency (ms)	2.9 ± 0.5
20–80% rise time (ms)	5.0 ± 0.2
Decay time constant (ms)	107.0 ± 5.0

LTP induced by high-frequency stimulation (HFS)[1]

Condition	Value (% of baseline)	Number of cells	P
HFS control	200 ± 21	12	0.0002
HFS + D-AP5 (20 µM, bath application)	98 ± 11	6	0.01
HFS + EGTA (20 mM, intracellular)	102 ± 11	5	0.003
HFS + nimodipine (10 µM, bath application)	82 ± 8	5	0.0007
HFS + QX-314 (10 mM, intracellular)	99 ± 11	6	0.008
HFS + TTX (20 nM, bath application)	98 ± 16	5	0.002

LTP induced by pairing of pre- and postsynaptic activity[2]

Condition	Value (% of baseline)	Number of cells	P
STDP (+10 ms) control	178 ± 22	9	0.004
STDP (+10 ms) D-	101 ± 5.	7	0.01

AP5 (20 µM, bath application)			
STDP (+10 ms) EGTA (20 mM, intracellular)	102 ± 7	8	0.007
STDP (+10 ms) nimodipine (10 µM, bath application)	91 ± 6	5	0.01
STDP (–10 ms) control	148 ± 12	15	0.0004
STDP (–10 ms) D-AP5 (20 µM, bath application)	101 ± 4	6	0.006
STDP (–10 ms) EGTA (20 mM, intracellular)	103 ± 21	5	0.018
STDP (–10 ms) nimodipine (10 µM, bath application)	105 ± 6	5	0.019
Presynaptic stimulation only	108 ± 6	5	0.19
Postsynaptic APs only	93 ± 8	5	0.44

1 The HFS protocol consisted of 4 trains of 100 stimuli at 100 Hz delivered every 10 s.
2 The pairing protocol consisted of 300 repetitions of a single presynaptic stimulation paired with a postsynaptic AP at different time intervals at 1 Hz.
All data shown in table were obtained at room temperature.

Table 2: Parameters of the pattern completion model.

Parameter	Explanation	Default value or range
n	Number of neurons	3,000
p	Connection probability	0.5
a	Total activity level	0.1
g_1	Inhibition factor	0 – 1
m	Pattern load (number of patterns applied in storage phase)	0 – 200
b_1	Proportion of valid firings in initial phase of recall (b_1 = 1 → identity to initial pattern)	0.5
b_n	Proportion of spurious firings in initial phase of recall (b_n = 1 → no spurious firing)	1
σ_t	Standard deviation of spike times in activity patterns	0.2 cycles
τ_{pot}	Synaptic potentiation time constant in the STDP rule	1 cycle
τ_{syn}	Synaptic decay time constant	1 cycle

For details, see Methods and Gibson and Robinson, 1992; Bennett et al., 1994.

4 Discussion

CA3–CA3 recurrent synapses play a key role in learning and memory (Nakazawa et al., 2002). However, little is known about the properties of synaptic plasticity at these synapses in acute hippocampal slices. The results obtained in the present study reveal noncanonical plasticity rules at glutamatergic CA3–CA3 recurrent synapses. First, HFS induces cooperative LTP. Voltage-gated Na^+ channels are required for HFS induced LTP but axosomatic spiking seems not to be essential. This result suggests that dendritic spikes may be involved in the induction of LTP at CA3–CA3 recurrent synapses. Second, an associative (pairing) protocol induces potentiation irrespective of the order of pairing. Increasing the time interval between pre–postsynaptic activities results in a temporally symmetric spike timing-dependent plasticity window with a maximum potentiation at +10 ms and minimum at ±100 ms. Further, in our autoassociative network model, the new STDP rule resulted in an increased storage capacity with improved reliability of pattern completion (Marr, 1971). Thus, induction of synaptic plasticity with a broad range of activity patterns at CA3–CA3 recurrent synapses may facilitate the storage of information.

4.1 Mechanisms of HFS-induced cooperative LTP at CA3–CA3 synapses

HFS is a classical paradigm for LTP induction and is shown to be particularly effective for LTP induction at many synapses (Bliss and Lømo, 1973; Zalutsky and Nicoll, 1990). We found that HFS efficiently induces LTP at CA3–CA3 recurrent synapses. The induction of LTP by HFS depended on the activation of NMDA-type glutamate receptors is in line with the previous studies (Harris and Cotman, 1986; Zalutsky and Nicoll, 1990). Further involvement of L-type Ca^{2+} channels in LTP induction suggests that there are at least two Ca^{2+} sources, one through postsynaptic NMDARs and the other through L-type Ca^{2+} channels. Our results with the slow intracellular Ca^{2+} chelator EGTA confirms that LTP induction leads to an influx of Ca^{2+} within the dendritic spines (Lynch et al., 1983; Malenka et al., 1988, 1992). These results also have implications

for the coupling distance between Ca^{2+} source and plasticity sensor (Lisman et al., 2012). Influx of Ca^{2+} following activation of NMDARs results into a region near the inner mouth of the channel called Ca^{2+} nanodomain (Schneggenburger and Neher, 2005). Ca^{2+} concentration in this region is very high. This increased Ca^{2+} then diffuses into the bulk of the spine head within microseconds. Since the process of diffusion of Ca^{2+} to the bulk of the spine is extremely fast, only a fast Ca^{2+} buffer (BAPTA) can block Ca^{2+} elevation in the nanodomain. On the other hand, either a fast or a slow buffer can block Ca^{2+} elevation in the bulk of the spine head. The effect of EGTA suggests that LTP induction at CA3–CA3 recurrent synapses is triggered by microdomains (spine head) rather than nanodomain (Eggermann et al., 2012; Hoffman et al., 2002). Thus, postsynaptic NMDARs and the molecular machinery for LTP induction seem to be spatially segregated within the compartment of a dendritic spine.

4.2 Requirement of Na^{+} channels for HFS-LTP induction

Removal of Mg^{2+} block of NMDAR requires postsynaptic depolarization which in turn leads to Ca^{2+} influx required for hebbian LTP to occur (Malenka and Nicoll, 1999). There are at least three different mechanisms by which postsynaptic depolarization could be achieved. First, postsynaptic AP reaches the spines retrogradely as the bAP (Stuart and Sakmann, 1994). The time-dependent association of EPSP and bAP cooperatively activates NMDARs to achieve LTP induction (Magee and Johnston, 1997; Markram et al., 1997; Stuart and Sakmann, 1994; Yuste and Denk, 1995). Second, localized passive synaptic depolarization itself is sufficient enough for depolarization (Bliss and Lømo, 1973). Third, localized passive synaptic depolarization is not able to generate sufficient depolarization instead activates dendritic spikes (Kim et al., 2015).

Interestingly, our results show that postsynaptic APs are not strictly required for HFS-induced LTP. Thus, initiation of axosomatic APs does not appear to be the mechanism underlying LTP induction. However, application of the intracellular Na^{+} channel blocker QX-314 or low concentration of TTX abolished LTP induction completely. The most likely interpretation of these data is that voltage-

gated Na^+ channels are blocked by channel blockers (QX-314 and TTX) and thereby suppress dendritic spikes in CA3 pyramidal neurons (Kim et al., 2012) which, in turn, abolishes LTP induction (Kim et al., 2015). Thus, the uniquely high level of excitability of CA3 pyramidal neurons and the abundance of dendritic spikes (Kim et al., 2012) may explain the specific properties of HFS induced LTP at CA3–CA3 recurrent synapses.

4.3 A novel form of STDP rule at CA3–CA3 recurrent synapses

In this study we have identified a novel STDP induction rule at CA3–CA3 recurrent synapses. The new STDP rule is temporally symmetric and does not show any long-term depression (LTD). This finding is different from previously reported STDP rules at other synapses which are all temporally asymmetric (Feldman, 2012). Similar to the HFS-induced LTP both blockers of NMDARs and L-type Ca^{2+} channels block STDP. These findings suggest that two independent Ca^{2+} sources are required for induction of LTP at these synapses (Magee and Johnston, 1997; Nevian and Sakmann, 2006). Spine $[Ca^{2+}]$ transients mediated by NMDARs and L-type Ca^{2+} channels show temporally symmetric summation when compared for different pairing time intervals. Thus, the properties of spine Ca^{2+} signaling may provide a mechanistic explanation for the temporally symmetric plasticity rule.

bAPs function as associative signals in STDP induction (Kampa et al., 2007; Sjöström et al., 2008). Local application of TTX to stop bAPs to propagate to the synapse can prevent LTP induction (Magee and Johnston, 1997). In a pre–postsynaptic activity sequence, bAPs provide the depolarization needed for activation of the NMDAR and the subsequent Ca^{2+} influx necessary for LTP induction (Kampa et al., 2004). This mechanism may also operate in CA3–CA3 synapses. An active AP backpropagation caused by the high dendritic Na^+ channel density in these cells (Kim et al., 2012) may be particularly effective. What could be the possible mechanism for post–presynaptic pairing? One possibility would be after-depolarization (ADP; Metz et al., 2005, 2007; Brown and Randall, 2009), a hallmark of CA3 pyramidal neuron excitability. What makes ADP suitable as an associative signal? ADP propagates into dendrites

without attenuation and it effectively summates with subsequent EPSPs (Kim, unpublished data). These properties enable a post–presynaptic sequence in CA3 neurons to produce large compound depolarizations. This depolarization would be particularly effective in removal of Mg^{2+} block and subsequent activation of NMDARs and voltage-gated Ca^{2+} channels. These summation properties appear to be specific for CA3 pyramidal neurons, since in layer 5 neocortical cells APs shunt subsequent EPSPs, rather than boosting their amplitude (Häusser et al., 2001).

One caveat with our symmetric STDP rule at CA3–CA3 synapses is the lack of depression (LTD). How is the stability achieved in the absence of a compensatory mechanism? Several additional regulatory mechanisms may be at work in the absence of depression. For example, homeostatic plasticity at CA3–CA3 synapses may counteract saturation in the network (Turrigiano and Nelson, 2004; Mitra et al., 2011). Homeostatic plasticity at mossy fiber synapses on CA3 pyramidal neurons could be an alternative or additional mechanism (Lee et al., 2013). Finally, LTD has been reported in CA3 pyramidal neurons early in development (Lei et al., 2003; Ho et al., 2007). Whether and how such LTD mechanisms can be reactivated in the mature brain remains to be determined.

Our autoassociative network model shows that the novel STDP rule enhances the computational power of the network. The storage capacity and the reliability of pattern completion (Marr, 1971) is increased. The temporally symmetric STDP rule addresses two major issues of previous models. First, it solves the problem that synchronous activity in ensembles generates LTD via a post–presynaptic sequence, because the time for dendritic propagation is shorter than that for axonal propagation of the AP (Kim et al., 2012). Second, it addresses how autoassociative network models can work under conditions of slightly asynchronous activity in CA3 pyramidal neuron ensembles. In particular, the broad and temporally symmetric STDP rule could be useful for the reactivation of cell assembly patterns of freely moving animals in open fields (O'Neill et al., 2008), and for the incorporation of contralateral CA3 pyramidal neurons into long-range neuronal assemblies.

4.4 Implications for network function

Diverse glutamatergic synapses are reported to show temporally asymmetric learning rules (Markram et al., 1997; Magee and Johnston, 1997; Bi and Poo, 1998; Feldman, 2012). The asymmetric learning rules are highly suitable for the learning of temporal sequences related to places or events in hippocampal networks (Abbott and Blum, 1996). What could be the function of temporally symmetric learning rules, as observed in CA3–CA3 cell recurrent synapses? CA3 pyramidal neurons are activated by the dentate gyrus via hippocampal mossy fiber synapses, which have a detonator / teacher function in the circuit (Henze et al., 2002; Bischofberger et al., 2006; Vyleta and Jonas, 2014). If we assume STDP rule to be asymmetric, mossy fiber activation would result in a post–presynaptic activity sequence, since dendritic AP backpropagation in CA3 pyramidal axon dendrites (Kim et al., 2012) will be faster than AP forward propagation in axons. This will result into long-term depression at CA3–CA3 recurrent synapses. In contrast, with the temporally symmetric STDP rule described in the present study, potentiation of glutamatergic synapses would occur. Additionally, the broadness of the STDP window may compensate for jitter in the AP timing of coactive cells in neuronal assemblies. This could be useful for the reactivation of cell assembly patterns acquired in open fields (O'Neill et al., 2008) and for pattern completion, a major function of the CA3 region (Marr, 1971; McNaughton and Morris, 1987). Broad, temporally symmetric STDP rules may be also relevant to strengthen synapses between CA3 cells in different hemispheres, which will show longer synaptic latencies and larger temporal jitter. Thus, the specific rules of induction of synaptic plasticity at CA3–CA3 recurrent synapses will translate into a unique capacity for storage of information in the CA3 cell network.

5 References

1. Abbott, L.F., Blum, K.I. Functional significance of long-term potentiation for sequence learning and prediction. *Cereb. Cortex* **6**, 406–416 (1996).

2. Andersen, P. Organization of hippocampal neurons and their interconnections. In R.L. Isaacson & K.H. Pribram (Eds.) *The Hippocampus*, 155-175 (1975).

3. Andersen, P., Morris, R., Amaral, D.G., Bliss, T., O'Keefe, J. *The hippocampus book*. *Oxford university press, Newyork* (2007).

4. Amaral, D.G., Ishizuka, N., Claiborne, B. Neurons, numbers and the hippocampal network. *Prog Brain Res.* **83**, 1-11 (1990).

5. Amaral, D.G., Witter, M.P. Hippocampal formation. In: Paxinos G, editor. *The rat nervous system* **2** (1995).

6. Ashby, M.C., De La Rue, S.A., Ralph, G.S., Uney, J., Collingridge, G.L., Henley, J.M. Removal of AMPA receptors (AMPARs) from synapses is preceded by transient endocytosis of extrasynaptic AMPARs. *J. Neurosci.* **24**, 5172–5176 (2004).

7. Benke, T.A., Luthi, A., Isaac, J.T., Collingridge, G.L. Modulation of AMPA receptor unitary conductance by synaptic activity. *Nature* **393**, 793–797 (1998).

8. Bennett, M.R., Gibson, W.G. & Robinson, J. Dynamics of the CA3 pyramidal neuron autoassociative memory network in the hippocampus. *Philos. Trans. R. Soc. Lond. B Biol. Sci.* **343**, 167–187 (1994).

9. Bi, G. & Poo, M.M. Synaptic modifications in cultured hippocampal neurons: Dependence on spike timing, synaptic strength, and postsynaptic cell type. *J. Neurosci.* **18**, 10464–10472 (1998).

10. Bischofberger J, Engel D, Li L, Geiger JR, Jonas P. Patch-clamp recording from mossy fiber terminals in hippocampal slices. *Nat Protoc.* **1**, 2075–2081 (2006).

11. Blackstad, T.W., Brink, K., Hem, J., Jeune, B. Distribution of hippocampal mossy fibers in the rat. An experimental study with silver impregnation methods. *J Comp. Neurol.* **138**, 433–449 (1970).

12. Blanpied, T.A., Scott, D.B., Ehlers, M.D. Dynamics and regulation of clathrin coats at specialized endocytic zones of dendrites and spines. *Neuron* **36**, 435–449 (2002).

13. Bliss, T.V., Lømo, T. Long-lasting potentiation of synaptic transmission in the dentate area of the anaesthetized rabbit following stimulation of the performant path. *J. Physiol.* **232**, 331–356 (1973).

14. Bliss, T.V., Collingridge, G.L. A synaptic model of memory: long-term potentiation in the hippocampus. *Nature* **7**, 361–369 (1993).

15. Blitzer, R.D., Connor, J.H., Brown, G.P., Wong, T., Shenolikar, S., Iyengar, R. Gating of CaMKII by cAMP-regulated protein phosphatase activity during LTP. *Science* **280**, 1940–1942 (1998).

16. Bolshakov, V.Y., Siegelbaum, S.A. Postsynaptic induction and presynaptic expression of hippocampal long-term depression. *Science* **264**, 1148–1152 (1994).

17. Bredt, D.S., Nicoll, R.A. AMPA receptor trafficking at excitatory synapses. *Neuron* **40**, 361–379 (2003).

18. Brown, J.T., Randall, A.D. Activity-dependent depression of the spike after-depolarization generates long-lasting intrinsic plasticity in hippocampal CA3 pyramidal neurons. *J. Physiol.* **587**, 1265–1281 (2009).

19. Cajal, S.R. Histology of the nervous system of man and vertebrates (Swanson N, Swanson L, translators)*. Oxford: Oxford University Press*, (1991).

20. Celikel, T., Szostak, V.A., and Feldman, D.E. Modulation of spike timing by sensory deprivation during induction of cortical map plasticity. *Nat. Neurosci.* **7**, 534–541 (2004).

21. Chicurel, M.E., Harris, K.M. Three-dimensional analysis of the structure and composition of CA3 branched dendritic spines and their synaptic relationships with mossy fiber boutons in the rat hippocampus. *J. Comp. Neurol.* **325**, 169–182 (1992).

22. Citri, A., Malenka, R.C. Synaptic plasticity: multiple forms, functions, and mechanisms. Neuropsychopharmacology. *Epub.* **33**, 18–41 (2008).

23. Claiborne, B.J., Amaral, D.G., Cowan, W.M. A light and electron microscopic analysis of the mossy fibers of the rat dentate gyrus. *J. Comp. Neurol.* **246**, 435–458 (1986).

24. Claiborne BJ, Amaral DG, Cowan WM. Quantitative, three-dimensional analysis of granule cell dendrites in the rat dentate gyrus. *J. Comp. Neurol*. **302**, 206-219 (1990).

25. Clugnet, M.C., LeDoux, J.E. Synaptic plasticity in fear conditioning circuits: induction of LTP in the lateral nucleus of the amygdala by stimulation of the medial geniculate body. *J. Neurosci.* **10**, 2818–2824 (1990).

26. Collingridge, G.L., Isaac, J.T., Wang, Y.T. Receptor trafficking and synaptic plasticity. *Nat. Rev. Neurosci.* **5**, 952–962 (2004).

27. Cummings, J.A., Mulkey, R.M., Nicoll, R.A., Malenka, R.C. Ca^{2+} signaling requirements for long-term depression in the hippocampus. *Neuron* **16**, 825–833 (1996).

28. Debanne, D., Gähwiler, B.H., Thompson, S.M. Long-term synaptic plasticity between pairs of individual CA3 pyramidal cells in rat hippocampal slice cultures. *J. Physiol.* **507**, 237–247 (1998).

29. Denk, W., Sugimori, M., Llinas, R. Two types of calcium response limited to single spines in cerebellar Purkinje cells. *PNAS* **92**, 8279–8282 (1995).

30. Derkach, V.A., Oh, M.C., Guire, E.S., Soderling, T.R. Regulatory mechanisms of AMPA receptors in synaptic plasticity. *Nat. Rev. Neurosci* **8**, 101–113 (2007).

31. Dudek, S.M., and Bear, M.F. Homosynaptic long-term depression in area CA1 of hippocampus and effects of N-methyl-D-aspartate receptor blockade. *PNAS* **89**, 4363–4367 (1992).

32. Eichenbaum, H. The hippocampus and declarative memory: cognitive mechanisms and neural codes. *Behav. Brain Res.* **127**,199–207 (2001).

33. Feldman, D.E. Timing-based LTP and LTD at vertical inputs to layer II/III pyramidal cells in rat barrel cortex. *Neuron* **27**, 45–56 (2000).

34. Feldman, D.E. The spike-timing dependence of plasticity. *Neuron* **75**, 556–571 (2012).

35. Fino, E., Glowinski, J., and Venance, L. Bidirectional activity-dependent plasticity at corticostriatal synapses. *J. Neurosci.* **25**, 11279–11287 (2005).

36. Fino, E., Deniau, J.M., and Venance, L. Cell-specific spike-timingdependent plasticity in GABAergic and cholinergic interneurons in corticostriatal rat brain slices. *J.Physiol.* **586**, 265–282 (2008).

37. Fino, E., Paille, V., Deniau, J.M., and Venance, L. Asymmetric spike timing-dependent plasticity of striatal nitric oxide-synthase interneurons. *Neuroscience* **160**, 744–754 (2009).

38. Froemke, R.C., Poo, M.M. & Dan, Y. Spike-timing-dependent synaptic plasticity depends on dendritic location. *Nature* **434**, 221–225 (2005).

39. Frotscher, M., Seress, L., Schwerdtfeger, W.K., Buhl, E. The mossy cells of the fascia dentata: a comparative stuy of their fine structure and synaptic connections in rodents and primates. *J. Comp. Neurol.* **312**,145–163 (1991).

40. Gibson, W.G. & Robinson, J. Statistical analysis of the dynamics of sparse associative memory. *Neural Networks* **5**, 645–661 (1992).

41. Giese, K.P., Fedorov, N.B., Filipkowski, R.K., Silva, A.J. Autophosphorylation at Thr286 of the alpha calcium-calmodulin kinase II in LTP and learning. *Science* **279**, 870–873 (1998).

42. Gonzales, R.B., DeLeon Galvan, C.J., Rangel, Y.M., Claiborne, B.J. Distribution of thorny excrescences on CA3 pyramidal neurons in the rat hippocampus. *J. Comp. Neurol.* **430**, 357–368 (2001).

43. Groc, L., Heine, M., Cognet, L., Brickley, K., Stephenson, F.A., Lounis, B. Differential activity-dependent regulation of the lateral mobilities of AMPA and NMDA receptors. *Nat. Neurosci* **7**, 695–696 (2004).

44. Grover, L.M., Teyler, T.J. Differential effects of NMDA receptor antagonist APV on tetanic stimulation induced and calcium induced potentiation. *Neurosci. Lett.* **113**, 309–314 (1990).

45. Guzman, S.J., Schlögl, A. & Schmidt-Hieber, C. Stimfit: quantifying electrophysiological data with Python. *Front Neuroinform.* **8**, 16 (2014a).

46. Guzman, S.J., Frotscher, M. & Jonas, P. Properties of CA3-CA3 synapses optimize storage capacity in the CA3 microcircuit. *Soc. of Neurosci. Abstr.* 302.11/C33 (2014b).

47. Han, V.Z., Grant, K., and Bell, C.C. Reversible associative depression and nonassociative potentiation at a parallel fiber synapse. *Neuron* **27**, 611–622 (2000).

48. Harris, E.W., Cotman, C.W. Long-term potentiation of guinea pig mossy fiber responses is not blocked by N-methyl D-aspartate antagonists. *Neurosci Lett.* **70**,132–137, (1986).

49. Hebb, D.O. The organization of behavior. *John Wiley & Sons, New Jersey, USA*, (1949).

50. Henze DA, Urban NN, Barrionuevo G. The multifarious hippocampal mossy fiber pathway: a review. *Neuroscience* **98**(3), 407–427 (2000).

51. Henze, D.A., McMahon, D.B., Harris, K.M., Barrionuevo, G. Giant miniature EPSCs at the hippocampal mossy fiber to CA3 pyramidal cell synapse are monoquantal. *J. Neurophysiol*. **1**, 15–29 (2002).

52. Heynen, A.J., Abraham, W.C., Bear, M.F. Bidirectional modification of CA1 synapses in the adult hippocampus in vivo. *Nature* **381**, 163–166 (1996).

53. Ho, M.T., Pelkey, K.A., Topolnik, L., Petralia, R.S., Takamiya, K., Xia, J., Huganir, R.L., Lacaille, J.C. & McBain, C.J. Developmental expression of Ca^{2+}-permeable AMPA receptors underlies depolarization-induced long-term

depression at mossy fiber CA3 pyramid synapses. *J. Neurosci.* **27**, 11651–11662 (2007).

54. Hoffman, D.A., Sprengel, R., Sakmann, B. Molecular dissection of hippocampal theta-burst pairing potentiation. *PNAS* **99**, 7740–7745 (2002).

55. Hopfield, J.J. Neural networks and physical systems with emergent collective computational abilities. *PNAS* **79**, 2554–2558 (1982).

56. Hrabetova, S., Sacktor, T.C. Bidirectional regulation of protein kinase M zeta in the maintenance of long-term potentiation and long-term depression. *J. Neurosci.* **16**, 5324–5333 (1996).

57. Ishizuka, N., Weber, J., Amaral, D.G. Organization of intrahippocampal projections originating from CA3 pyramidal cells in the rat. *J. Comp. Neurol.* **295**, 580–623 (1990).

58. Kamiya, H., Shinozaki, H. & Yamamoto, C. Activation of metabotropic glutamate receptor type 2/3 suppresses transmission at rat hippocampal mossy fibre synapses. *J. Physiol.* **493**, 447–455 (1996).

59. Kalia, L.V., Gingrich, J.R., Salter, M.W. Src in synaptic transmission and plasticity. *Oncogene* **23**, 8007–8016 (2004).

60. Kampa, B.M., Clements, J., Jonas, P. & Stuart, G.J. Kinetics of Mg^{2+} unblock of NMDA receptors: implications for spike-timing dependent synaptic plasticity. *J. Physiol.* **556**, 337–345 (2004).

61. Kampa, B.M., Letzkus, J.J. & Stuart, G.J. Dendritic mechanisms controlling spike-timing-dependent synaptic plasticity. *Trends Neurosci.* **30**, 456–463 (2007).

62. Kemp A, Manahan-Vaughan D. Hippocampal long-term depression: master or minion in declarative memory processes? *Trends Neurosci.* **30**, 111–118 (2007).

63. Kim, S., Guzman, S.J., Hu, H. & Jonas, P. Active dendrites support efficient initiation of dendritic spikes in hippocampal CA3 pyramidal neurons. *Nat. Neurosci.* **15**, 600–606 (2012).

64. Kim. Y., Hsu, C.L., Cembrowski, M.S., Mensh, B.D., Spruston, N. Dendritic sodium spikes are required for long-term potentiation at distal synapses on hippocampal pyramidal neurons. *eLife* **4**, e06414 (2015).

65. Kirkwood, A., Bear, M.F. Homosynaptic long-term depression in the visual cortex. *J Neurosci* **14**, 3404–3412 (1994).

66. Kobayashi K, Manabe T, Takahashi T. Presynaptic long-term depression at the hippocampal mossy fiber-CA3 synapse. *Science* **273**, 648–650 (1996).

67. Koester, H.J., Sakmann, B. Calcium dynamics in single spines during coincident pre– and postsynaptic activity depend on relative timing of back-propagating action potentials and subthreshold excitatory postsynaptic potentials. *PNAS*. **95**, 9596–9601 (1998).

68. Lee K.J., Queenan, B.N., Rozeboom, A.M., Bellmore, R., Lim, S.T., Vicini, S. & Pak, D.T. Mossy fiber-CA3 synapses mediate homeostatic plasticity in mature hippocampal neurons. *Neuron* **77**, 99–114 (2013).

69. Lei, S., Pelkey, K.A., Topolnik, L., Congar, P., Lacaille, J.C. & McBain, C.J. Depolarization-induced long-term depression at hippocampal mossy fiber-CA3 pyramidal neuron synapses. *J. Neurosci.* **23**, 9786–9795 (2003).

70. Li, X.G., Somogyi, P., Ylinen, A. & Buzsáki, G. The hippocampal CA3 network: an in vivo intracellular labeling study. *J. Comp. Neurol.* **339**, 181–208 (1994).

71. Lisman, J. A mechanism for the Hebb and the anti-Hebb processes underlying learning and memory. *PNAS* **86**, 9574–9578 (1989).

72. Lisman, J.E. Relating hippocampal circuitry to function: recall of memory sequences by reciprocal dentate-CA3 interactions. *Neuron* **22**, 233–242 (1999).

73. Lisman, J., Yasuda, R., Raghavachari, S. Mechanisms of CaMKII action in long-term potentiation. *Nat. Rev. Neurosci.* **13**, 169–82 (2012).

74. Levy, W.B., Steward, O. Temporal contiguity requirements for long-term associative potentiation/depression in the hippocampus. *Neuroscience* **8**, 791–797 (1983).

75. Letzkus, J.J., Kampa, B.M. & Stuart, G.J. Learning rules for spike timing-dependent plasticity depend on dendritic synapse location. *J. Neurosci.* **26**, 10420–10429 (2006).

76. Lu, J.T., Li, C.Y., Zhao, J.P., Poo, M.M., and Zhang, X.H. Spike-timing dependent plasticity of neocortical excitatory synapses on inhibitory interneurons depends on target cell type. *J. Neurosci.* **27**, 9711–9720 (2007).

77. Lynch, M.A. Long-term potentiation and memory. *Physiol Rev* **84**: 87–136 (2004).

78. MacVicar, B.A., Dudek, F.E. Local synaptic circuits in rat hippocampus: interactions between pyramidal cells. *Brain Res*. **184**, 220–223 (1980).

79. Magee, J.C. & Johnston, D. A synaptically controlled, associative signal for Hebbian plasticity in hippocampal neurons. *Science* **275**, 209–213 (1997).

80. Makhinson, M., Chotiner, J.K., Watson, J.B., O'Dell, T.J. Adenylyl cyclase activation modulates activity-dependent changes in synaptic strength and

Ca^{2+}/calmodulin-dependent kinase II autophosphorylation. *J. Neurosci.* **19**, 2500–2510 (1999).

81. Malenka, R.C., Kauer, J.A., Perkel, D.J., Mauk, M.D., Kelly, P.T., Nicoll, R.A. An essential role for postsynaptic calmodulin and protein kinase activity in long-term potentiation. *Nature* **340**, 554–557 (1989).

82. Malenka, R.C., Nicoll, R.A. Long-term potentiation- a decade of progress? *Science* **285**, 1870–1874 (1999).

83. Malenka, R.C., Bear, M.F. LTP and LTD: an embarrassment of riches. *Neuron* **44**, 5–21(2004).

84. Malenka, R.C., Nicoll, R.A. NMDA-receptor-dependent synaptic plasticity: multiple forms and mechanisms. *Trends in Neurosci.* **16**, 521–527(1993).

85. Malinow, R., Schulman, H., Tsien, R.W. Inhibition of postsynaptic PKC or CaMKII blocks induction but not expression of LTP. *Science* **245**, 862–866 (1989).

86. Malinow, R., Malenka, R.C. AMPA receptor trafficking and synaptic plasticity. *Annu Rev Neurosci* **25**, 103–126 (2002).

87. Markram, H., Lübke, J., Frotscher, M. & Sakmann, B. Regulation of synaptic efficacy by coincidence of postsynaptic APs and EPSPs. *Science* **275**, 213215 (1997).

88. Marr, D. Simple memory: a theory for archicortex. *Philos. Trans. R. Soc. Lond. B Biol. Sci.* **262**, 23–81 (1971).

89. Martin, S.J., Grimwood, P.D., Morris, R.G. Synaptic plasticity and memory: an evaluation of the hypothesis. *Annu. Rev. Neurosci.* **23**, 649–711(2000).

90. Masukawa, L.M., Benardo, L.S., Prince, D.A. Variations in electrophysiological properties of hippocampal neurons in different subfields. *Brain Res.* **242**, 341–344 (1982).

91. McNaughton, B.L. & Morris, R.G.M. Hippocampal synaptic enhancement and information storage within a distributed memory system. *Trends Neurosci.* **10**, 408–415 (1987).

92. Mayford, M., Bach, M.E., Huang, Y.Y., Wang, L., Hawkins, R.D., Kandel, E.R. Control of memory formation through regulated expression of a CaMKII transgene. *Science* **274**, 1678–83 (1996).

93. Metz, A.E., Jarsky, T., Martina, M. & Spruston, N. R-type calcium channels contribute to afterdepolarization and bursting in hippocampal CA1 pyramidal neurons. *J. Neurosci.* **25**, 5763–5773 (2005).

94. Metz, A.E., Spruston, N. & Martina, M. Dendritic D-type potassium currents inhibit the spike afterdepolarization in rat hippocampal CA1 pyramidal neurons. *J. Physiol.* **15**, 175–187 (2007).

95. Miles, R., Wong, R.K. Single neurones can initiate synchronized population discharge in the hippocampus. *Nature* **306**, 371–373(1983).

96. Miles, R. & Wong, R.K.S. Excitatory synaptic interactions between CA3 neurones in the guinea-pig hippocampus. *J. Physiol.* **373**, 397–418 (1986).

97. Milner B, Squire LR, Kandel ER. Cognitive neuroscience and the study of memory. *Neuron* **20**, 445–468 (1998).

98. Mitra, A., Mitra, S.S. & Tsien, R.W. Heterogeneous reallocation of presynaptic efficacy in recurrent excitatory circuits adapting to inactivity. *Nat. Neurosci.* **15**, 250–257 (2011).

99. Montgomery, J.M., Pavlidis, P. & Madison, D.V. Pair recordings reveal all-silent synaptic connections and the postsynaptic expression of long-term potentiation. *Neuron* **29**, 691–701 (2001).

100. Morishita, W., Connor, J.H., Xia, H., Quinlan, E.M., Shenolikar, S., Malenka, R.C. Regulation of synaptic strength by protein phosphatase 1. *Neuron* **32**, 1133–1148 (2001).

101. Morris, R.G. Elements of a neurobiological theory of hippocampal function: the role of synaptic plasticity, synaptic tagging and schemas. *Eur. J. Neurosci.* **23**, 2829–2846 (2006).

102. Morris, R.G., Frey, U. Hippocampal synaptic plasticity: role in spatial learning or the automatic recording of attended experience? *Philos. Trans. R. Soc. Lond.* **352**, 1489–1503 (1997).

103. Mulkey, R.M., Malenka, R.C. Mechanisms underlying induction of homosynaptic long-term depression in area CA1 of the hippocampus. *Neuron* **9**, 967–975 (1992).

104. Mulkey, R.M., Herron, C.E., Malenka, R.C. An essential role for protein phosphatases in hippocampal long-term depression. *Science* **261**, 1051–1055 (1993).

105. Mulkey, R.M., Endo, S., Shenolikar, S., Malenka, R.C. Involvement of a calcineurin/inhibitor-1 phosphatase cascade in hippocampal long-term depression. *Nature* **369**, 486–488 (1994).

106. Nakazawa, K., Quirk, M.C., Chitwood, R.A., Watanabe, M., Yeckel, M.F., Sun, L.D., Kato, A., Carr, C.A., Johnston, D., Wilson, M.A. & Tonegawa, S. Requirement for hippocampal CA3 NMDA receptors in associative memory recall. *Science* **297**, 211–218 (2002).

107. Nicoll, R.A. Expression mechanisms underlying long-term potentiation: a postsynaptic view. *Philos. Trans. R. Soc. Lond.* **358**, 721–726 (2003).

108. Nicoll, R.A., Malenka, R.C. Contrasting properties of two forms of long-term potentiation in the hippocampus. *Nature* **14**, 377–378 (1995b).

109. Nevian, T. & Sakmann, B. Spine Ca^{2+} signaling in spike-timing-dependent plasticity. *J. Neurosci.* **26**, 11001–11013 (2006).

110. Normann, C., Peckys, D., Schulze, C.H., Walden, J., Jonas, P. & Bischofberger, J. Associative long-term depression in the hippocampus is dependent on postsynaptic N-type Ca^{2+} channels. *J. Neurosci.* **20**, 8290–8297 (2000).

111. Oertner, T.G., Sabatini, B.L., Nimchinsky, E. & Svoboda, K. Facilitation at single synapses probed with optical quantal analysis. *Nat. Neurosci.* **5**, 657–664 (2002).

112. O'Keefe J, Dostrovsky J. The hippocampus as a spatial map. Preliminary evidence from unit activity in the freely-moving rat. *Brain Res.* **34**, 171–175 (1971).

113. Oliet, S.H., Malenka, R.C., Nicoll, R.A. Two distinct forms of long-term depression coexist in CA1 hippocampal pyramidal cells. *Neuron* **18**, 969–982 (1997).

114. O'Neill, J., Senior, T.J., Allen, K., Huxter, J.R. & Csicsvari, J. Reactivation of experience-dependent cell assembly patterns in the hippocampus. *Nat. Neurosci.* **11**, 209–215 (2008).

115. Otani, S., Connor, J.A. Requirement of rapid Ca^{2+} entry and synaptic activation of metabotropic glutamate receptors for the induction of long-term depression in adult rat hippocampus. *J. Physiol. (Lond)* **511**, 761–770 (1998).

116. Pastalkova, E., Serrano, P., Pinkhasova, D., Wallace, E., Fenton, A.A., Sacktor, T.C. Storage of spatial information by the maintenance mechanism of LTP. *Science* **313**, 1141–1144 (2006).

117. R. Lorente, de. Nó Studies on the structure of the cerebral cortex. II. Continuation of the study of ammonic system. *J. Psychol. Neurol.* **46**, 113–177 (1934).

118. Rolls, E. T., Treves, A.. Neural Networks and Brain Function. *Oxford: Oxford University Press* (1998)

119. Ropireddy, D., Scorcioni, R., Lasher, B., Buzsáki, G. & Ascoli, G.A. Axonal morphometry of hippocampal pyramidal neurons semi-automatically reconstructed after in vivo labeling in different CA3 locations. *Brain Struct. Funct.* **216**, 1–15 (2011).

120. Safo, P., Regehr, W.G. Timing dependence of the induction of cerebellar LTD. *Neuropharmacology* **54**, 213–218 (2008).

121. Schacter, Daniel L; Gilbert, Daniel T; Wegner, Daniel M; (2010). *Implicit Memory and Explicit Memory Psychology*, New York: Worth Publishers.

122. Schaffer, K. Beitrag zur Histologie der Ammonshornformation. *Arch. Mikroskop. Anatomie* **39***,* 611–632 (1892)*.*

123. Schindelin, J., Arganda-Carreras, I., Frise, E., Kaynig, V., Longair, M., Pietzsch, T., Preibisch, S., Rueden, C., Saalfeld, S., Schmid, B., Tinevez, J.Y., White, D.J., Hartenstein, V., Eliceiri, K., Tomancak, P. & Cardona, A. Fiji: an open-source platform for biological-image analysis. *Nat. Methods* **9**, 676–682 (2012).

124. Schneggenburger, R. & Neher, E. Presynaptic calcium and control of vesicle fusion. *Curr. Opin. Neurobiol.* **15**, 266–274 (2005).

125. Scoville WB, Milner B. Loss of recent memory after bilateral hippocampal lesions. 1957. *J Neuropsychiatry Clin. Neurosci.* **12**, 103–113 (2000).

126. Selig, D.K., Hjelmstad, G.O., Herron, C., Nicoll, R.A., Malenka, R.C. Independent mechanisms for long-term depression of AMPA and NMDA responses. *Neuron* **15**, 417–426 (1995).

127. Serrano, P., Yao, Y., Sacktor, T.C. Persistent phosphorylation by protein kinase Mzeta maintains late-phase long-term potentiation. *J. Neurosci.* **25**, 1979–1984 (2005).

128. Shen, W., Flajolet, M., Greengard, P., and Surmeier, D.J. Dichotomous dopaminergic control of striatal synaptic plasticity. *Science* **321**, 848–851 (2008).

129. Siegelbaum, S.A., Kandel, E.R. Learning-related synaptic plasticity: LTP and LTD. *Curr. Opin. Neurobiol.* **1**, 113–120 (1991).

130. Silva, A.J., Paylor, R., Wehner, J.M., Tonegawa, S. Impaired spatial learning in alpha-calcium-calmodulin kinase II mutant mice. *Science* **257**, 206–211 (1992).

131. Sjöström, P.J., Turrigiano, G.G. & Nelson, S.B. Rate, timing, and cooperativity jointly determine cortical synaptic plasticity. *Neuron* **32**, 1149–1164 (2001).

132. Sjöstrom, P.J., and Hausser, M. A cooperative switch determines the sign of synaptic plasticity in distal dendrites of neocortical pyramidal neurons. *Neuron* **51**, 227–238 (2006).

133. Sjöström, P.J., Rancz, E.A., Roth, A. & Häusser, M. Dendritic excitability and synaptic plasticity. *Physiol. Rev.* **88**, 769–840 (2008).

134. Soderling, T.R., Derkach, V.A. Postsynaptic protein phosphorylation and LTP. *Trends Neurosci.* **23**, 75–80 (2000).

135. Song, I., Huganir, R.L. Regulation of AMPA receptors during synaptic plasticity. *Trends Neurosci.* **25**, 578–588 (2002).

136. Squire, L.R. Memory systems of the brain: a brief history and current perspective. *Neurobiol. Learn. Mem.* **82**, 171–177 (2004).

137. Squire, L.R. The legacy of patient H.M. for neuroscience. *Neuron*. **61**, 6-9 (2009).

138. Stuart, G.J., Sakmann, B. Active propagation of somatic action potentials into neocortical pyramidal cell dendrites. *Nature* **367**, 69–72 (1994).

139. Swanson, L.W., Wyss, J.M.,Cowan, W.M. An autoradiographic study of the organization of the efferent connections of the hippocampal formation in the rat. *J. Comp. Neurol.* **181**, 681–715 (1978).

140. Sweatt, J.D. Mitogen-activated protein kinases in synaptic plasticity and memory. *Curr. Opin. Neurobiol.* **14**, 311–317 (2004).

141. Tang, Y.P., Shimizu, E., Dube, G.R., Rampon, C., Kerchner, G.A., Zhuo, M. et al Genetic enhancement of learning and memory in mice. *Nature* **401**, 63–69 (1999).

142. Thomas, G.M., Huganir, R.L. MAPK cascade signalling and synaptic plasticity. *Nat. Rev. Neurosci* **5**, 173–183 (2004).

143. Treves, A. & Rolls, E.T. Computational analysis of the role of the hippocampus in memory. *Hippocampus* **4**, 374–391 (1994).

144. Tulving, Episodic and semantic memory. In Organization of Memory, ed. E Tulving, W Donaldson, *New York: Academic,* 381–403 (1972).

145. Turrigiano, G.G. & Nelson, S.B. Homeostatic plasticity in the developing nervous system. *Nat. Rev. Neurosci.* **5**, 97–107 (2004).

146. Tzounopoulos, T., Janz, R., Südhof, T.C., Nicoll, R.A., Malenka, R.C. A role for cAMP in long-term depression at hippocampal mossy fiber synapses. *Neuron* **4**, 837–845 (1998).

147. Witter, M.P. Intrinsic and extrinsic wiring of CA3: indications for connectional heterogeneity. *Learn Mem.***14**, 705-713 (2007)

148. Yuste, R., Denk, W. Dendritic spines as basic functional units of neuronal integration. *Nature* **375**, 682-684 (1995).

149. Zalutsky, R.A. & Nicoll, R.A. Comparison of two forms of long-term potentiation in single hippocampal neurons. *Science* **248**, 1619–1624 (1990).

150. Zhang, J.C., Lau, P.M., and Bi, G.Q. Gain in sensitivity and loss in temporal contrast of STDP by dopaminergic modulation at hippocampal synapses. PNAS **106**, 13028–13033 (2009).

151. Zhang, LI., Tao, H.W., Holt, C.E., Harris, W.A., Poo, M. A critical window for cooperation and competition among developing retinotectal synapses. Nature **395**, 37–44 (1998).

152. Zilberter, M., Holmgren, C., Shemer, I., Silberberg, G., Grillner, S., Harkany, T., and Zilberter, Y. Input specificity and dependence of spike-timingdependent plasticity on preceding postsynaptic activity at unitary connections between neocortical layer 2/3 pyramidal cells. *Cereb. Cortex* **19**, 2308–2320 (2009).

6 Publication

Symmetric spike timing-dependent plasticity at CA3–CA3 synapses optimizes storage and recall in autoassociative networks

Rajiv K. Mishra, Sooyun Kim[1], Segundo J. Guzman[2] & Peter Jonas[2]

IST Austria (Institute of Science and Technology Austria), Am Campus 1, A-3400 Klosterneuburg, Austria

1 Present address: Department of Physiology, Seoul National University College of Medicine, 103 Daehak-ro, Jongno-gu Seoul, 110-799, Republic of Korea

2 Equal contribution; correspondence should be addressed to either S.J.G. or P.J.

Corresponding authors:

Dr. Peter Jonas

Dr. Segundo J. Guzman

IST Austria (Institute of Science and Technology Austria)

Am Campus 1

A-3400 Klosterneuburg

Austria

Phone: ++43-2243-9000-3700

Fax: ++43-2243-9000-2007

E-mail: peter.jonas@ist.ac.at

E-mail: jose.guzman@ist.ac.at